Analytical Solutions to the Stochastic Kinetic Equation for Liquid and Ice Particle Size Spectra. Part II: Large-Size Fraction in Precipitating Clouds

Vitaly I. Khvorostyanov

Central Aerological Observatory, Dolgoprudny, Moscow Region, Russian Federation

Judith A. Curry

School of Earth and Atmospheric Sciences, Georgia Institute of Technology, Atlanta, Georgia

(Manuscript received XX Month 2007, in final form XX Month 2007)

Corresponding author address:

Dr. J. A. Curry
School of Earth and Atmospheric Sciences
Georgia Institute of Technology
Phone: (404) 894-3948
Fax: (404) 894-5638
curryja@eas.gatech.edu

Abstract

The stochastic kinetic equation is solved analytically for precipitating particles that can be identified with rain, snow, and graupel. The general solution for the size spectra of the large-size particles is represented by the product of an exponential term and a term that is an algebraic function of radius. The slope of the exponent consists of the Marshall-Palmer slope and an additional integral that is a function of radius. Both the integral and algebraic term depend on the condensation and accretion rates, vertical velocity, turbulence coefficient, terminal velocity of the particles, and the vertical gradient of the liquid (ice) water content. At sufficiently large radii, the radius dependence of the algebraic term is a power law, and the spectra have the form of gamma distributions. Simple analytical expressions are derived for the slopes and indices of the size distributions. These solutions provide explanations of the observed dependencies of the cloud particle spectra in different phases and size regimes on temperature, height, turbulence, vertical velocities, liquid or ice water content, and other cloud properties. These analytical solutions and expressions for the slopes and shape parameters can be used for parameterization of the spectra of precipitating particles and related quantities (e.g., optical properties, radar reflectivities) in bulk cloud microphysical parameterizations and in remote sensing techniques.

1. Introduction

Parameterizations of the size spectra $f_l(r)$ of precipitating cloud particles (rain, snow, graupel, etc.) in the form of the Marshall-Palmer (1948, hereafter MP) and Gunn-Marshall (1958) exponential distributions,

$$f_l(r) = N_0 \exp(-\beta_l r), \quad (1.1)$$

where β_l is the slope and N_0 is the intercept, are widely used in cloud physics and routinely incorporated into bulk cloud models and remote sensing techniques (see review, e.g., in Cotton and Anthes 1989). More recently, three parameter gamma distributions were suggested as a better alternative for rain and snow size spectra (e.g., Ulbrich 1983; Willis 1984; Heymsfield 2003)

$$f_l(r) = c_N r^{p_l} \exp(-\beta_l r), \quad (1.2)$$

where r is the particle radius, p_l is the index of the gamma distribution (shape parameter), positive or negative, and c_N is the coefficient determined from the normalization to the concentration or mass density. The exponential MP distribution (1.1) is a particular case of (1.2) with $p_l = 0$, whereby (1.2) is a more general form that allows the additional degrees of freedom. Equations (1.1), (1.2) are often formulated in terms of diameters D, $f_l(D)$~exp(-ΛD), with the slope $\Lambda = \beta_l/2$.

Earlier theoretical studies of the size spectra of precipitating particles were directed towards explaining the exponential shape of the MP spectra and evolution of its parameters. Golovin (1963), Scott (1968), Srivastava and Passarelli (1980), and Voloshchuk (1984) determined analytical solutions to the kinetic equation of condensation and coagulation with some idealized assumptions: homogeneous kernels of the coagulation integral and some non-Maxwellian models for the condensation growth rate; some of these solutions were in the form of exponential functions (1.1). Srivastava (1971) hypothesized that a balance exists between the collision-coalescence and spontaneous breakup of raindrops, which leads to the exponential MP spectra, but the derived slopes were distinctly steeper than the observed spectra. Passarelli (1978a,b) assumed that the snow spectra are described by the MP spectrum and found an analytical expression for the slopes via integral moments by solving the stochastic collection equation without account for breakup. Passarelli's model with exponential spectra was further developed and generalized by a number of authors (e.g., Mitchell 1994, Mitchell et al. 1996). Verlinde et al. (1990) obtained a closed form for the analytical solution to the collection growth equation for the original size spectra described by gamma distributions (1.2).

Subsequently it became clear that collisional rather than spontaneous breakup may be more important in restricting drop growth and formation of the observed raindrop exponential spectra (see review, e.g., in Pruppacher and Klett 1997, hereafter PK97). Srivastava (1978) formulated a simplified model of collisional breakup with a fixed constant number of fragments as a variable parameter and developed a parameterization for raindrop spectra in the form of general exponential but with time varying Λ and N_0. Low and List (1982a,b, hereafter LL82) developed a complex empirical parameterization of the fragment distribution function for collisional drop breakup. The parameterization of LL82 has been used in many numerical solutions of the stochastic coalescence/breakup equation to explain the mechanism of formation of the MP spectra and their slopes (e.g., Feingold et al 1988; Hu and Srivastava 1995; Brown 1991, 1997; McFarquhar 2004; Seifert 2005).

These numerical solutions produced somewhat different equilibrium size spectra but with common features. The spectra were characterized by the following: a small size region from ~ 200 μm to ~2 mm consisting of several peaks with shallow troughs between them, the first peak occurring near diameter ~ 200-300 μm with an abrupt decrease at sizes smaller 200 μm that determine the lower limit r_0 of the large-size fraction; and a region beginning at ~2 -2.5 mm and comprising the MP exponential tail. McFarquhar (2004) refined the LL82 equations and emphasized that measurement and sampling problems impose uncertainties on the solutions, motivating more detailed laboratory studies and improved parameterizations.

The numerical studies focused on analyzing the positions of the peaks and values of the slopes but did not attempt to approximate the entire rain spectrum by gamma distributions and to determine the index p_l, which is widely used in cloud models and remote sensing of rain and snow and typically rather arbitrarily prescribed. Parameterization of the large particle size spectrum in the form of the gamma distribution (1.2) has been undertaken by many empirical studies that were directed toward determination of the 3 parameters of the spectra, and in particular of the index p_l. Ulbrich (1983) found a correlation between the type of the rain and the index p_l; there was $p_l < 0$ for orographic rain indicating broad spectra, and $0 < p_l < 2$ for thunderstorm rain indicating narrower spectra. For widespread and stratiform rain, p_l was more variable but mostly positive. Willis (1984) found the best value $p_l \approx 2.5$ for raindrops from two hurricanes.

More recently, another type of p_l dependence was suggested, a Λ - p_l relation, whereby Λ was expressed as a quadratic polynomial of p_l or vice versa (e.g., Zhang et al. 2001, 2003a,b; Brandes et al. 2003). The validity of this parameterization was tested in direct simulations of convective rains with the cloud models using the LL82 kernel (e.g. Seifert 2005). The Λ - p_l relation allows reduction of the number of independent parameters in (1.1) to two but the general dependence of the index p_l on the rain type described by Ulbrich (1983) is still unclear. A similar relation was suggested by Heymsfield (2003) for crystalline clouds.

Previous research has revealed some fundamental properties of the size spectra of precipitating particles, and has shed some light on the mechanisms of their formation. However, direct application of these findings in cloud models and remote sensing retrievals meets the following problems: owing to the complexity of collision/breakup kernels, to our knowledge, only numerical solutions of the stochastic coalescence/breakup kinetic equation have been obtained for realistic representations of the gravitational kernel. The numerical solutions require small time steps of 0.1-1 s, are rather time consuming, and do not provide simple analytical parameterizations for the indices and slopes of the exponential and gamma distributions that are needed in cloud and climate models and remote sensing retrievals.

In Khvorostyanov and Curry (1999a,b, hereafter KC99a,b) and Khvorostyanov and Curry (2008, hereafter Part I), gamma distributions were derived for the small-size fraction as the solutions of the kinetic equation of stochastic condensation. The goal of this paper (Part II) is to obtain analytical solutions of the stochastic kinetic equation for precipitating cloud particles and to explain observed variations in the size spectra that can be used to parameterize the size spectra for modeling and remote sensing applications. The paper is organized as follows. In section 2, the basic stochastic kinetic equation is given, and assumptions and simplifications are described. Section 3 presents the general solutions and 4 particular cases are considered: the size range where fallspeed is a linear function of particle size; the size range where fall speed is proportional to the square root of particle size; conditions where coagulation growth is dominant; and the subcloud layer with no small-size fraction. In section 4, a physical interpretation is given for these solutions and they are illustrated for a crystalline cloud. Conclusions are formulated in section 5.

2. Basic equation and assumptions

As in Part 1, we consider either pure liquid or crystalline clouds; mixed phase is not considered here. The entire size spectrum of the drops or crystals consists of two size fractions, small, $f_s(r)$, and large, $f_l(r)$, with the boundary radius at $r = r_0$ between the two size fractions, where a minimum is usually observed in the size spectra composed of both fractions. Based on this minimum, the value $r_0 \sim$ 30-50 μm can be assumed for the liquid phase (see e.g., Fig. 4.3 in Cotton and Anthes 1989), and ~30-80 μm (or maximum dimension $D_0 \sim$ 60-160 μm) for the crystals as illustrated in section 4. The functions $f_s(r)$ and $f_l(r)$ correspond to the bulk categorization of the condensed phase into cloud water and rain for the liquid phase and cloud ice and snow for the crystalline phase.

The same assumptions as in Part 1 for the small-size fraction are made here for the large-size fraction size distribution function f_l: 1) horizontal homogeneity or horizontal averaging over some scale, so that horizontal derivatives are zero (the solutions can be easily generalized for the nonzero horizontal derivatives in parametric form); 2) quasi-steady state, so that $\partial f_l/\partial t = 0$. With these assumptions, the kinetic equation (2.6) from Part 1 can be written for the size distribution function of the large-size fraction f_l of the drops or crystals

$$\frac{\partial}{\partial z}[(w - v(r))f_l] + \frac{\partial}{\partial r}(\dot{r}_{cond} f_l) = k\frac{\partial^2 f_l}{\partial z^2}$$
$$+ c_n kG\left(\frac{\partial^2 f_l}{\partial r \partial z} + \frac{\partial^2 f_l}{\partial z \partial r}\right) + c_{nn} kG^2 \frac{\partial^2 f_l}{\partial r^2} + \left(\frac{\partial f}{\partial t}\right)_{col,ls}$$
$$+ \left(\frac{\partial f}{\partial t}\right)_{col,g} + \left(\frac{\partial f}{\partial t}\right)_{col,l} + \left(\frac{\partial f}{\partial t}\right)_{br,g} + \left(\frac{\partial f}{\partial t}\right)_{br,l} \qquad (2.1)$$

Here z is height, r is the particle radius, k is the coefficient of turbulent diffusion, w is the vertical velocity, $v(r)$ is the particle fall velocity, $\dot{r}_{cond}$ is the condensation (deposition) growth rate; a dimensionless parameter G and c_n, c_{nn}, are the coefficients arising from the nonconservative turbulence coefficients k_{ij}^{n}, k_{ij}^{nn} defined in Part 1. The first 3 terms on the right-hand side describe the turbulent transport and effects of stochastic condensation. The 4th term, $(\partial f_l/\partial t)_{col,ls}$, is collection gain in the large-size fraction due to coagulation (accretion) with the small-size fraction, and the terms $(\partial f_l/\partial t)_{col,g}$, $(\partial f_l/\partial t)_{col,l}$, $(\partial f_l/\partial t)_{br,g}$, $(\partial f_l/\partial t)_{br,l}$ denote respectively collection gain, collection loss, breakup gain, and breakup loss due to interactions within the large-size fraction alone. Such decomposition of the collection terms is similar to that in Srivastava (1978).

Simplified Maxwellian growth rate is assumed for condensation/deposition

$$\dot{r}_{cond} = \frac{bS}{r}, \qquad b = \frac{D_v \rho_{vs}}{\Gamma_p \rho_w}, \qquad (2.2)$$

where D_v is the vapor diffusion coefficient, Γ_p is the psychrometric correction to the growth rate associated with the latent heat of condensation, ρ_w is the water (ice) density, $S = (\rho_v - \rho_{vs})/\rho_{vs}$ is supersaturation over water or ice, ρ_v and ρ_{vs} are the environmental and saturated over water (ice) vapor densities.

Continuous collection approximation is assumed for $(\partial f_l/\partial t)_{col,ls}$. In this approximation, only the collision-coalescence between the particles of the different fractions of the spectrum, $f_s(r)$ and $f_l(r)$, is considered, i.e., small particles are collected by large particles. The continuous collection approximation is used usually for evaluation of the accretion rate of the large-size fraction as in Kessler's (1969) and subsequent works. If it appears in formulation of kinetic equations, the corresponding term $(\partial f_l/\partial t)_{col,ls}$ is usually written without derivation by analogy with the Maxwellian growth, with the growth rate of individual particles $(dr/dt)_{coag}$ or $(dm/dt)_{coag}$ defined in the continuous collection approximation (e.g., Cotton and Anthes 1989; PK97). This approach is intuitively clear, but its accuracy and relation to the full Smoluchowski stochastic collection equation is not clear.

Therefore, the derivation of continuous collection approximation from the integral Smoluchowski collection equation and simplifications are given in Appendix A. It is shown there that: 1) the continuous collection approximation is *a first order approximation by the mass of the small particle* to the full stochastic coagulation equation; 2) the Smoluchowski coagulation equation allows in this approximation significant simplifications, the term $(\partial f_l/\partial t)_{col,ls}$ for the collection gain can be written analogously to the condensation term (the 2nd term on the left-hand side in (2.1)):

$$\left(\frac{\partial f_l(r)}{\partial t}\right)_{col,ls} = -\frac{\partial}{\partial r}[\dot{r}_{coag} f_l(r)] = -\chi \frac{\partial}{\partial r}[v(r) f_l], \qquad (2.3)$$

where $\dot{r}_{coag}$ is the accretion radius growth rate

$$\dot{r}_{coag} = \dot{m}_{coag} \frac{dr}{dm} = \chi v(r), \qquad \chi = \frac{E_c q_{ls}}{4\rho_w}. \qquad (2.4)$$

Now, the integral Smoluchowski coagulation equation can be written in the continuous collection approximation in a simplified differential form for both small and large fractions as

$$\left(\frac{\partial f_{s,l}(r)}{\partial r}\right)_{col} = -\chi \frac{\partial}{\partial r}[v(r) f_l]\theta(r - r_0) - \sigma_{col} f_s(r)\theta(r_0 - r), \qquad (2.5)$$

where $\theta(x)$ is the Heaviside step function. The first term is the reduced gain for the large-size fraction. The second term is reduced loss for the small size fraction; σ_{col} is the same collection rate as introduced in (2.5) of Part I and used there in calculations of small-size spectra; it is derived in Appendix A here:

$$\sigma_{col} = \pi E_c \int_{r_0}^{\infty} r^2 v(r) f_l(r) dr \, . \qquad (2.6)$$

This form of σ_{col} ensures mass conservation, i.e., the mass loss of small fraction is equal to the mass gain of the large fraction. We can introduce also the inverse quantity,

$$\tau_{col} = \sigma_{col}^{-1} = \left(\pi E_c \int_{r_0}^{\infty} r^2 v(r) f_l(r) dr \right)^{-1}, \qquad (2.7)$$

which is the characteristic accretion time of the e-folding decrease in q_{ls} or increase in q_{ll} if the other processes are absent. It is interesting to compare this time scale with the supersaturation relaxation time τ_p discussed in Part 1

$$\tau_p = \left(4\pi D_v \int_0^{\infty} r[f_s(r) + f_l(r)] dr \right)^{-1} = [4\pi D_v (N_s \bar{r}_s + N_l \bar{r}_l)]^{-1}, \qquad (2.8)$$

where $\bar{r}_s$, $\bar{r}_l$ are the mean radii of the small and large-size fraction, N_l is the number density of the large-size fraction. This time determines the condensation (evaporation) growth rate. The term $N_s \bar{r}_s$ is usually greater than $N_l \bar{r}_l$, thus the time τ_p at condensation is determined mostly by the small particles; in the absence of small particles at evaporation, τ_p is determined by the large fraction. The accretion time τ_{col} is determined by the large particles as follows from (2.7).

If the cloud water content of the large-size fraction is small enough, the last 4 terms in (2.1), $(\partial f_l/\partial t)_{col,g}$, $(\partial f_l/\partial t)_{col,l}$, $(\partial f_l/\partial t)_{br,g}$, $(\partial f_l/\partial t)_{br,l}$ for collection and breakup are also small and can be neglected, which is usually done in most bulk cloud models. This situation corresponds to sufficiently small concentrations N_l of the large drops, so that collisions among large particles are not frequent. With increasing N_l, water content and rain or snow intensity, the error of this approximation may increase and these terms should be accounted for; this is especially important for convective clouds. Srivastava (1982) and Feingold et al. (1988) evaluated the coalescence and breakup terms analytically, but the collision and breakup kernels were specified to be constant (independent of radii), and the solution was expressed via Bessel functions that are difficult to analyze analytically.

We use a parameterization of coalescence and breakup based on an assumption that is justified using the work by Hu and Srivastava (1995, hereafter HS95). The detailed analysis of various terms in the coalescence-breakup kinetic equation [the last 4 terms in (2.1)] performed in HS95 showed that these terms are: a) approximately proportional to each other over the major radii range, and b) are mostly mutually compensated near the equilibrium steady state. We hypothesize that these terms are proportional to the accretion gain $(\partial f_l/\partial t)_{col,ls}$ and can be roughly parameterized by expressing via $(\partial f_l/\partial t)_{col,ls}$ with some proportionality coefficients $c_{cg} > 0$, $c_{cl} < 0$, $c_{bg} > 0$, $c_{bl} < 0$ for the corresponding processes ("c" and "b" mean collection and breakup; "g" and "l" mean gain and loss). These coefficients are, in general, functions of r but are proportional to each other. Therefore the sum of $(\partial f_l/\partial t)_{col,ls}$ and all 4 last terms in (2.1) can be expressed via $(\partial f_l/\partial t)_{col,ls}$ as

$$c_{cb}\left(\frac{\partial f}{\partial t}\right)_{col,ls}, \qquad (2.9)$$

where $c_{cb} = 1 + c_{cg} + c_{cl} + c_{bg} + c_{bl}$. In a box model used in HS95, equilibrium among these 4 terms is reached after some sufficient time so that they are mutually compensated, forming equilibrium spectra, thus, $c_{cb} \to 1$. In our case, the balance includes also vertical mass gradient, and diffusion and accretion growth, so that there can be only partial compensation among the above 4 terms, and c_{cb} can slightly differ from 1. That is, the net effect of collection and breakup gain and loss is to change the accretion growth rate $\dot{r}_{coag}$ of the large particles described by (2.4), i.e., the collection efficiency E_c. Then we can introduce the correction c_{cb} into parameter E_c and solve the equation with account for only $(\partial f_l/\partial t)_{col,ls}$ as in (2.3). This corresponds to the approximation adopted in most bulk cloud models. It will be shown below that this simple parameterization yields the functional r-dependence of collection growth rate that is in a good agreement with more precise calculations in HS95.

Note that the assumption (2.9) is not mandatory for analytical solutions obtained below, we just use the fact, based on HS95, that the sum of these 4 terms caused by interactions within only large fraction can be much smaller (due to mutual compensation) than the term $(\partial f_l/\partial t)_{col,ls}$ caused by interactions between the small and large fractions. When the numerical models provide new information about the relative values of the terms in coagulation-breakup equation, this assumption and analytical solutions can be modified accordingly.

The same closure as in Part 1 is chosen for the vertical gradient of the size spectra

$$\frac{\partial f_l(r,z)}{\partial z} = \alpha_l(z)\varsigma_l(r) f_l(r,z). \qquad (2.10)$$

In the simplest model $\zeta_l(r) = 1$, α_l can be related from (2.10) to the relative gradient of the LWC (IWC) of the large-size fraction:

$$\alpha_l(z) = (1/q_{ll})(dq_{ll}/dz), \qquad (2.11)$$

Substituting (2.10) into (2.1) allows elimination of z- derivatives; using also (2.2), (2.4), and assuming in this work $\zeta_l(r) = 1$, we have a differential equation that is a function only of r:

$$c_{nn}kG^2 \frac{d^2 f_l}{dr^2} + \left[-\frac{bS}{r} - \chi v(r)\right]\frac{df_l}{dr}$$

$$+\left[\alpha_l^2 k + \frac{d(\alpha_l k)}{dz} - \alpha_l (w - v) - \frac{dw}{dz} + \frac{bS}{r^2} - \chi \frac{dv(r)}{dr}\right] f_l = 0 . \tag{2.12}$$

3. Solutions for the large-size fraction with account for diffusion growth and coagulation

We seek analytical solutions for the general case and then for particular cases that include the size range where fallspeed is a linear function of particle size; fallspeed is proportional to the square root of particle size; conditions where coagulation growth is dominant; and in the subcloud layer with no small-size fraction.

3.1 General solution

The previous solutions in sections 3, 4 of Part 1 indicate that stochastic condensation may influence predominantly the small-size fraction. Therefore, it is reasonable to assume that the contribution of the stochastic diffusion terms are much smaller for the large-size fraction, and shape of the spectra is determined mostly by the balance between regular growth/evaporation, vertical transport, collection, and sedimentation. Then neglecting in (2.12) the terms with G and the effects of stochastic condensation, and using (2.10), (2.11), the kinetic equation can be written for the quasi-steady state as

$$bS \frac{d}{dr}\left(\frac{f_l}{r}\right) + \chi \frac{d}{dr}(f_l v(r)) + [w - v(r) - \alpha_l k]\alpha_l f_l = 0 , \tag{3.1}$$

(we neglect here for simplicity the terms with dw/dz, dk/dz , $d\alpha_l/dz$ that can be introduced into the final equations).

Introducing a new variable $\varphi_l = f_l/r$, and solving (3.1) relative to φ_l, we obtain

$$\frac{1}{\varphi_l} \frac{d\varphi_l}{dr} = -\psi(r) , \tag{3.2}$$

where

$$\psi(r) = \beta_{l0} + \frac{u(r)}{g(r)} + \frac{1}{g(r)} \frac{dg(r)}{dr} , \tag{3.3}$$

$$\beta_{l0} = -\frac{\alpha_l}{\chi}, \tag{3.4}$$

$$g(r) = bS + \chi r v(r) = r\dot{r}_{tot}(r), \tag{3.5}$$

$$u(r) = -\beta_{l0} bS + \alpha_l r(w - \alpha_l k), \tag{3.6}$$

where $\dot{r}_{tot}(r) = \dot{r}_{cond}(r) + \dot{r}_{coag}(r)$ is the total radius growth rate. The integral of (3.2) is

$$\varphi_l(r) = \varphi_l(r_0)\exp(-J_0), \qquad J_0 = \int_{r_0}^{r} \psi(r')dr', \tag{3.7}$$

where r_0 is the left boundary of the large-size fraction. Substituting (3.3) - (3.6) into (3.7), and integrating we obtain the solution for $f_l(r)$

$$f_l(r) = f_l(r_0)\frac{r}{r_0}\frac{g(r_0)}{g(r)}\exp[-\beta_{l0}(r - r_0) - J_{l1}]$$

$$= f_l(r_0)\frac{\dot{r}_{tot}(r_0)}{\dot{r}_{tot}(r)}\exp[-\beta_{l0}(r - r_0) - J_{l1}]. \tag{3.8}$$

where

$$J_{l1} = \int_{r_0}^{r} \frac{u(r')}{g(r')}dr'. \tag{3.9}$$

This is the general solution to the kinetic equation (3.1) for the large-size fraction at $r > r_0$ with account for the condensation and continuous collection. For application in bulk microphysical models, the integral J_{l1} can be evaluated numerically at any value of w, k, S, α_l, q_s; the fallspeeds $v(r)$ for the drops with account for nonsphericity and for various crystal habits can be evaluated as continuous functions of r following Bohm (1989), Mitchell (1996), Khvorostyanov and Curry (2002, 2005, hereafter KC02, KC05).

In certain particular cases, the integral J_1 can be obtained analytically and the solutions are simplified if the quasi-power law for terminal velocity

$$v(r) = A_v r^{B_v} \tag{3.10}$$

is applicable. Substituting (3.5), (3.6), and (3.10) into (3.9) and assuming that A_v =const and B_v = const over some interval of radii (r_1, r_2), we obtain

$$J_{l1} = I_1 + I_2 \,, \tag{3.11}$$

$$I_1 = -\beta_{l0} bS \int_{r_1}^{r_2} \frac{dr}{bS + \chi A_v r^{B_v+1}} \,, \tag{3.12a}$$

$$I_2 = \alpha_l (w - \alpha_l k) \int_{r_1}^{r_2} \frac{rdr}{bS + \chi A_v r^{B_v+1}} \,. \tag{3.12b}$$

Tabulated analytical expressions for these integrals exist only for very limited values of B_v (Gradshteyn and Ryzhik 1994). Therefore we will illustrate the general solution for three particular cases: 1) $v(r)$ is a linear function of r; 2) the case when the condensation rate is much smaller than the collection rate and can be neglected; and 3) $v(r)$ is proportional to $r^{1/2}$.

3.2. Particular case: fallspeed as a linear function of particle size

The linear regime for particle terminal velocity, $v(r) = A_v r$, is valid in the intermediate range of drop radius 60 to 600 μm (e.g. Rogers 1979), for spherical ice particles, and for some crystal habits in the region r = 90 - 300 μm (e.g., Mitchell 1996; KC02; KC05). The integrals I_1 and I_2 for the linear function $v(r)$ are evaluated in Appendix A. The integrals have different expressions for the cases of condensation ($S > 0$) and evaporation ($S < 0$) and can be expressed using the new parameters

$$R = \left(\frac{b\,|S|}{\chi A_v} \right)^{1/2} = r \left(\frac{|\dot{r}_{cond}(r)|}{\dot{r}_{coag}(r)} \right)^{1/2} \,, \tag{3.13a}$$

$$U = \beta_{l0} \frac{(\alpha_l k - w)}{2A_v} \,, \qquad Q = \frac{\beta_0 R}{2} \,, \tag{3.13b}$$

where $|S|$ and $|\dot{r}_{cond}|$ denote the absolute values of supersaturation and diffusion growth rates.

Substituting expressions for I_1 and I_2 at $S > 0$ from Appendix A into (3.12a,b) and then into (3.8) yields the following $f_l(r)$ in the condensation layer:

$$f_l(r) = f_l(r_0)\frac{\dot{r}_{tot}(r_0)}{\dot{r}_{tot}(r)}\left[\frac{(r_0/R)^2+1}{(r/R)^2+1}\right]^U$$

$$\times \exp\left[-\beta_{l0}(r-r_0) - \beta_{l0}R\left(\mathrm{arctg}\frac{r}{R} - \mathrm{arctg}\frac{r_0}{R}\right)\right], \qquad S > 0 . \qquad (3.14)$$

Using expressions for I_1 and I_2 from Appendix A for the evaporation layer ($S < 0$) yields 2 solutions for the two size regions, $r < R$ and $r > R$:

$$f_l(r) = f_l(r_0)\frac{\dot{r}_{tot}(r_0)}{\dot{r}_{tot}(r)}\left[\frac{(1+r/R)(1-r_0/R)}{(1-r/R)(1+r_0/R)}\right]^Q$$

$$\times\left[\frac{1-(r_0/R)^2}{1-(r/R)^2}\right]^U \exp[-\beta_{l0}(r-r_0)], \qquad S<0, \quad r<R . \qquad (3.15)$$

$$f_l(r) = f_l(r_0)\frac{\dot{r}_{tot}(r_0)}{\dot{r}_{tot}(r)}\left[\frac{(r_0/R-1)(r/R+1)}{(r_0/R+1)(r/R-1)}\right]^Q$$

$$\times\left[\frac{(r_0/R)^2-1}{(r/R)^2-1}\right]^U \exp[-\beta_{l0}(r-r_0)], \qquad S<0, \quad r>R . \qquad (3.16)$$

The physical meaning of the parameter R and of the solutions (3.14) - (3.16) is clear from (3.13a): $(r/R)^2 = \dot{r}_{coag}/|\dot{r}_{cond}|$ is the ratio of the collection rate to the condensation/evaporation rate. The conditions $r < R$ or $r > R$ mean that the condensation/evaporation rate is greater or smaller than the collection rate, $\dot{r}_{coag} < |\dot{r}_{cond}|$ or $\dot{r}_{coag} > |\dot{r}_{cond}|$. The boundary condition $r = R = (b|S|/\chi A_v)^{1/2}$ can be estimated for the following parameters: $T \sim 0$ ºC, $\rho_{vs} \approx 5\times10^{-6}$ g cm^{-3}, super- or subsaturation $S = \pm0.1$ (±10 %), $q_{ls} = 0.1$ g m^{-3}, $E_c = 0.5$, $A_v \approx 8\times10^3$ s^{-1} (from Rogers 1979). Then $\chi \sim 10^{-8}$, $b|S| \sim 10^{-7}$ cm^2 s^{-1}, and $R \sim 350$ µm. For $|S| = 0.2$ (±20 %), or $|S| = 0.4$ (±40 %), as can be in crystalline clouds or in evaporation layers, R increases to ~ 500 and 700 μm. With $|S| = 10^{-3}$ (± 0.1 %) and $q_{ls} = 1$ g m^{-3}, as in convective clouds, $R \sim 12 - 15$ μm at $T = 0$ to 10 ºC. For conditions of cirrus, T = -40 to -50 ºC, p = 200 hPa, q_{ls} = 20 mg m^{-3}, $|S| = 0.10$ (± 10 %), the value $R \sim 200$ μm. These estimates can be used to assess the asymptotic solutions.

The asymptotic at $r >> R$ is the same for both solutions (3.14) - (3.16) at sub- and supersaturations:

$$f_l(r) = f_l(r_0)\left(\frac{r}{r_0}\right)^{p_l} \exp[-\beta_0(r - r_0)]. \tag{3.17a}$$

$$p_l = -(2U + 1) = \beta_{l0}\frac{(w - \alpha_l k)}{A_v} - 1 \tag{3.17b}$$

Thus, the analytical solutions for the large-size fraction in both the growth and evaporation layers are gamma distributions similar to those suggested and analyzed by Ulbrich (1983), Willis (1984), Zhang et al. (2001, 2003a,b), Brandes (2003), Heymsfield (2003), and others.

If in (3.17b) the parameter $(2U+1) < 0$, then the index p_l is positive and the spectra represent the typical gamma distributions. If $(2U+1) > 0$, then the index p_l is negative, i.e., these generalized gamma spectra represent a product of the inverse power law of the Heymsfield-Platt (1984) type (hereafter, HP spectrum) and the exponential Marshall-Palmer spectrum. Which functional type dominates depends on the combination of the parameters. The condition $w > \alpha_l k$ usually takes place in (3.17b), and the term with w mostly determines p_l. As discussed in Part I, the effective w decreases with increasing scales of spatial-temporal averaging. At sufficiently large scales, w becomes small, p_l tends to zero and size spectrum (3.17a) tends to MP distribution. This prediction of our model coincides with the observations (e.g. Joss and Gori 1978), and statistical theories of MP spectra (e.g., Liu 1993). However, the local spectra can be narrower than the MP's, and better described by gamma distributions like (3.17a) as discussed in Introduction. Which type of the spectrum is preferable and what can be a relation between β_l and p_l is still the subject of discussion in the literature, see section 4.

3.3 Particular case: quasi-power law for the terminal velocity and $\dot{r}_{coag} >> \dot{r}_{cond}$

For sufficiently large *r* and small sub- or supersaturations, when $\dot{r}_{coag} >> \dot{r}_{cond}$, the condensation rate can be neglected. Then, using the quasi-power law form (3.10) for the fallspeed $v(r)$, assuming A_v and B_v are approximately constant in some region of *r* and $B_v < 1$, the integral J_{l1} in (3.9) can be evaluated as

$$J_{l1} = \beta_{l0}(\alpha_l k - w)\int_{r_0}^{r} \frac{dr}{v(r)} = \beta_{l0}\left(\frac{w-\alpha_l k}{1-B_v}\right)\left(\frac{r}{v(r)} - \frac{r_0}{v(r_0)}\right). \quad (3.18)$$

Introducing a size dependent slope $\beta_l(r)$

$$\beta_l(r) = \beta_{0l}\left[1 + \frac{w-\alpha_l k}{(1-B_v)v(r)}\right], \quad (3.19)$$

and substituting (3.18) with (3.19) into (3.8), we obtain

$$f_l(r) = f_l(r_0)\frac{v(r_0)}{v(r)}\exp\{-[\beta_l(r)r - \beta_l(r_0)r_0]\}. \quad (3.20)$$

Assuming that $B_v \approx$ const in the considered region of *r*, (3.20) becomes

$$f(r) = f(r_0)\left(\frac{r}{r_0}\right)^{-B_v}\exp[-\beta(r)(r-r_0)]. \quad (3.21)$$

Thus, we obtain again a generalized gamma distribution with the negative index $p_l = -B_v$. This is again a product of the Heymsfield-Platt and Marshall-Palmer size distributions; which dependence dominates, depends on the combination of the parameters. In most cloud types, $v(r) >> w$ and $v(r) >> \alpha_l k$ for the large-size fraction, then $\beta(r) \approx \beta_{l0}$ and

$$f(r) = c_N\left(r/r_0\right)^{-B_v}\exp(-\beta_{l0}r). \quad (3.22)$$

Since $B_v \le 0.5$ for large particles, the spectrum tends to the Marshall-Palmer exponent, however, there is also an algebraic term that is a function of *r*.

3.4 Particular case: fallspeed as $v(r) = A_v r^{1/2}$

For sufficiently large radii, the terminal velocity can be approximated by the law $v(r) = A_v r^{1/2}$ where A_v includes also a height correction $(\rho_{a0}/\rho_a)^{1/2}$ with ρ_{a0} and ρ_a being the air densities at the surface and at a given height (e.g., Rogers 1979, KC05). This regime is approximately valid for large drops, spherical ice particles (graupel, hail) and some other crystals habits. The integrals I_1 and I_2 in (3.12a,b) for this case with $B_v = 1/2$ are evaluated in Appendix B. Substituting them into J_{l1} in (3.8) yields for $S > 0$:

$$f_l(r) = f_l(r_0)\frac{\dot{r}_{tot}(r_0)}{\dot{r}_{tot}(r)}\left(\frac{x+1}{x_0+1}\right)^{2\Phi_1}\left(\frac{x^2-x+1}{x_0^2-x_0+1}\right)^{-\Phi_1}$$

$$\times\exp\left[-\beta_{l0}(r-r_0)-V(x-x_0)+\frac{2\beta_{l0}H}{\sqrt{3}}\arctan\frac{2x-1}{\sqrt{3}}\Bigg|_{x_0}^{x}+\frac{V}{\sqrt{3}}\arctan\frac{x\sqrt{3}}{2-x}\Bigg|_{x_0}^{x}\right], \quad (3.23)$$

where the vertical bar with limits is used in the same meaning as in the integrals and

$$x = \left(\frac{r}{H}\right)^{1/2}, \quad x_0 = \left(\frac{r_0}{H}\right)^{1/2} \quad H = \left(\frac{b|S|}{\chi A_v}\right)^{2/3}, \quad (3.24a)$$

$$V = \frac{2\alpha_l(w-\alpha_l k)H^{1/2}}{\chi A_v}, \quad \Phi_1 = \frac{V}{6} - \frac{\beta_{l0}H}{3}. \quad (3.24b)$$

Substitution of I_1 and I_2 for $S < 0$ from Appendix B into (3.8) yields

$$f_l(r) = f_l(r_0)\frac{\dot{r}_{tot}(r_0)}{\dot{r}_{tot}(r)}\left(\frac{x-1}{x_0-1}\right)^{-2\Phi_2}\left(\frac{x^2+x+1}{x_0^2+x_0+1}\right)^{\Phi_2}$$

$$\times\exp\left[-\beta_{l0}(r-r_0)-V(x-x_0)+\frac{2\beta_{l0}H}{\sqrt{3}}\arctan\frac{2x+1}{\sqrt{3}}\Bigg|_{x_0}^{x}+\frac{V}{\sqrt{3}}\arctan\frac{x\sqrt{3}}{2+x}\Bigg|_{x_0}^{x}\right], \quad (3.25)$$

$$\Phi_2 = \frac{V}{6} + \frac{\beta_{l0}H}{3} \quad (3.26)$$

The parameter H is here the characteristic length that determines the onset of the asymptotic regime. An estimate of H from (3.24a) with $q_{ls} = 0.1$ g m^{-3} (stratiform clouds) with b and ρ_{vs} at $T \sim 0$ºC, $|S| = 0.1$ (± 10%, ice phase), $A_v = 2.2\times10^3$ $(\rho_0/\rho)^{1/2}$ cm$^{1/2}$ s^{-1} (Rogers 1979) yields $H \approx 300$ μm. For the same q_{ls} but with $|S| = 10^{-3}$ (± 0.1%, liquid phase), $H \approx 15$ μm; with $q_{ls} \sim 1$ g m^{-3} (convective clouds), $H \sim 5$ μm. For cirrus at T = -40 to -50 ºC, $p \sim 200$ mb, $\rho/\rho_0 \sim 0.4$, and q_{ls} = 10 - 20 mg m^{-3}, an estimate yields $H \sim 60$ - 120 μm. Thus, in all these cases, $r >> H$, and $x >> 1$ for the large-size fraction. We can estimate the asymptotics of various terms in (3.23) at $x >> 1$. The product of two brackets with x before the exponent tends at large x to a limit $x^{2\Phi_1} x^{-2\Phi_1} \to 1$. The arguments of arctan in the exponent tend to infinity, arctan tend to $\pm\pi/2$, which results in a change of the normalizing constant. The term $1/\dot{r}_{tot}(r) \to r/[rv(r)] = v(r)^{-1/2} \to r^{-1/2}$. Incorporating these estimates, we find the asymptotic of $f_l(r)$ at $S > 0$

$$f_l(r) \sim r^{-1/2} \exp[-\beta_{l0} r - V(r/H)^{1/2}] \qquad (3.27)$$

The same estimates for f_l (3.25) at $S < 0$ yield the same asymptotic. An estimate of V with q_{ls} = 0.1 g m^{-3} and w = 1 cm s^{-1} gives $V \sim 0.1$. At $r \sim 1$ mm, the value $Vx \sim 0.3$, while with $\beta_{l0} \sim 40$ cm^{-1}, the value $\beta_{l0} r = 4$. Thus, the term Vx in the exponent of (3.27) can be neglected and $f_l(r) \sim r^{-1/2} \exp(-\beta_{l0} r)$, i.e., its asymptotic coincides with that in section 3.3 and tends to the Marshall-Palmer spectrum with a correction $r^{-1/2}$. However, for greater convective updrafts of $w \sim 1$ m s^{-1} and $\sim q_{ls}$ = 1 g m^{-3}, an estimate yields $V \sim 1$, i.e., the value $Vx \sim 3$ at $r \sim 1$ mm, which is comparable in magnitude to $\beta_{l0} r$. Then the term Vx should be retained in the exponent, the slope becomes nonlinear and the spectra may be slightly concave downward in log-linear coordinates (the slopes increase and the spectra decrease with r faster than for the MP spectrum) as observed by Willis (1984) in convective clouds.

3.5 Solution for subcloud layer

The previous solutions were obtained for the case of large particles co-existing with cloud liquid/ice (small-size fraction). When the small-size fraction has been evaporated (e.g., falling through the subsaturated subcloud layer, or in the downdraft or near the cloud edge), and large drops exist without the cloud particles, another regime occurs, $\dot{r}_{coag} << \dot{r}_{cond}$. To address this situation, we solve (3.1) with account for diffusional growth (evaporation) but neglecting the accretion term

$$bS\frac{d}{dr}\left(\frac{f_l}{r}\right)+[w-v(r)-\alpha_l k]\alpha_l f_l = 0\,. \tag{3.28}$$

This equation coincides with Eq. (4.1) of Part 1 for the tail of the small-size fraction, except that the loss term with σ_{col} is absent and we omitted for brevity the terms with dk/dz and $d\alpha_l/dz$ (which can be included into the final solution). Assuming again a power law for the terminal velocity with coefficients A_v, B_v, we can modify the solution (4.2) from Part 1 as:

$$f_l(r) = \frac{r}{r_{be}} f_l(r_{be})\exp\{-[\beta_{le}(r)r - \beta_{le}(r_{be})r_{be}]\}\,, \tag{3.29}$$

with r_{be} denotes the lower boundary of the large-size fraction, and the size-dependent slope $\beta_{le}(r)$ for the evaporation layer is

$$\beta_{le}(r) = \frac{r\alpha_l}{bS}\left(\frac{w-\alpha_l k}{2} - \frac{v(r)}{B_v+2}\right). \tag{3.30}$$

For large enough r and without vigorous vertical velocities, the 2nd term in (3.30) dominates and the slope is similar to that obtained in (4.7) of Part 1

$$\beta_{le}(r) = c_{l1} r v(r)\,, \qquad c_{l1} = -\frac{\alpha_l}{bS(B_v+2)} \tag{3.31}$$

To ensure a decrease of f_l with r, β_{le} should be positive; thus, the signs of α_l and S should be different in the evaporation layer, i.e., $\alpha_l > 0$ at $S < 0$, and LWC (IWC) should decrease downward in the subcloud layer that is characterized by evaporating precipitation.

The spectra in (3.29) are generalized gamma distributions and the functional behavior of the slopes depends on the velocity power index. In particular, $\beta_{le} \sim r^2$ and $f_l \sim \exp(-c_{l1}A_v r^3)$ for $v(r) = A_v r$ and $\beta_{le} \sim r^{3/2}$, $f_l \sim \exp(-c_{l1}A_v r^{5/2})$ for $v(r) = A_v r^{1/2}$. In vigorous downdrafts that cause subsaturation, such that $|w| >> v(r)$, the asymptotic slope (3.30) becomes

$$\beta_{le} = c_{l2} r\,, \qquad c_{l2} = \frac{\alpha_l (w - \alpha_l k)}{2bS}\,. \tag{3.32}$$

Since both w and S are negative, $\alpha_l > 0$, then $-\alpha_l k < 0$, $\beta_{le} > 0$ and (3.32) ensures a correct asymptotic. Then the spectrum behaves as $f_l \sim \exp(-c_{l2} r^2)$. Thus, the spectra of the precipitating particles in the evaporating subcloud layer fall off more rapidly with r than in the case with $q_{ls} > 0$, and become concave downward in log-linear coordinates, which can explain some observations described by Ulbrich (1983), Willis (1984), Zawadski and Agostinho (1988).

4. Interpretation of the solutions

In this section, a physical interpretation is given for the solutions in section 3 and they are illustrated with calculations for a crystalline cloud.

4.1 General analysis

The Marshall-Palmer spectra, $f_l \sim \exp(-\Lambda D)$, play a fundamental role in many cloud and climate models and remote sensing (especially radar) techniques. The values of $\Lambda = \beta_{l0}/2$ can be estimated using (3.4) for β_{l0} that can be rewritten for layers with $q_{ls} > 0$ by using (2.4) for χ

$$\beta_{l0} = \frac{4(-\alpha_l)\rho_w}{E_c q_{ls}}\,. \tag{4.1}$$

Note that $\alpha_l < 0$ since f_l and q_l increase downward, which is expected for falling particles growing by collection. Under this condition, $\beta_{l0} > 0$ and $\exp(-\beta_{l0} r)$ decreases with r. Eq. (4.1) reveals that β_{l0} decreases, i.e., the spectra stretch toward large-sizes, when the following processes occur :1) E_c or q_{ls} increase, i.e., the rate of mass transfer from the small to the large-size fraction increases; 2) ρ_w decreases and the mass gained by the large-size fraction is distributed over the larger range of volumes and radii; 3) $(-\alpha_l) = |\alpha_l|$ decreases, i.e., the gravitational, convective and turbulent fluxes of f_l decrease, causing weaker outflow of f_l from a given cloud level.

As an example, we can estimate from (4.1) the slope β_{l0} for the snow size spectra using data from Passarelli (1978b). Taking $E_c \sim 0.5$-1, snowflake bulk density $\rho_w \sim 0.1$ -0.2 g cm^{-3}, the water content of the small-size fraction as $q_{ls} \sim 0.1$ g m^{-3}, and thickness of the layer ~ 0.5 - 2 km, we obtain $\beta_{l0} \approx 40$ - 160 cm^{-1}, or $\Lambda = \beta_{l0}/2 \approx 20$ - 80 cm^{-1}. This is within the range of values of Λ = 10 - 100 cm^{-1} given by Passarelli (1978b), Houze et al. (1979), Platt (1997) and Ryan (2000).

Eq. (4.1) provides an explanation for some observed peculiarities of β_{l0} in crystalline clouds. The analyses performed by Houze et al. (1979), Platt (1997) and Ryan (2000) shows that β_{l0} increases by about an order of magnitude when temperature T decreases from 0 º C to -50 ºC (Fig. 3 in Platt 1997). The same analysis shows that the ice water content decreases in this temperature range, although somewhat faster (Fig. 4 in Platt 1997). According to (4.1), $\beta_{l0} \sim q_{ls}^{-1}$, and this may explain the observed increase in β_{l0} with decreasing T and q_{ls}. The slower increase with T by β_{l0} relative to the decrease in q_{ls} may be caused by decreasing cloud thickness at lower T, i.e., vertical gradients of IWC and α_l in the numerator of (4.1). This temperature dependence of β_{l0} or Λ may cause the height dependence observed by Passarelli (1978b), who measured $\Lambda \approx 65$ cm^{-1} at $z = 3.35$ km ($T = -20$ ºC) and $\Lambda \approx 24$ cm^{-1} at $z = 2.55$ km ($T = -12$ ºC). This increase in Λ (or β_{l0}) with decreasing height can be also a consequence of the $q_{ls}(T)$ dependence.

An interesting feature of the exponential MP spectra is that the range of slopes is similar for both liquid and crystalline particles. Marshall and Palmer (1948) give an equation $\Lambda = 41R_0^{-0.21}$ (cm^{-1}), with R_0 being the rainfall rate in mm h^{-1}, yielding $\beta_{l0} = 2\Lambda = 130$ to 50 cm^{-1} for $R_0 = 0.1$ to 10 mm h^{-1}. An estimate from (4.1) with $E_c \sim 0.5$, $\rho_w \sim 1$ g cm^{-3}, $q_{ls} \sim 1$ g m^{-3}, $\alpha_l \sim$ 0.5 km^{-1} yields $\beta_{l0} = 40$ cm^{-1}, which is in the middle of the range of β_{l0} values determined for the MP spectra and hence (4.1) can be applicable for MP spectra in liquid clouds.

Considering convective rain and the equations in section 3.2, the p_l- index (3.17b) with $v(r) = A_v r$ is applicable near the observed modal diameter ~0.2 - 0.4 mm in warm rain (e.g., Ulbrich 1983, Willis 1984). Using the relation $-\alpha_l = \beta_{l0}\chi$ from (3.4), (3.17b) can be written as

$$p_l = c_{\beta 1}\beta_{l0}^2 + c_{\beta 2}\beta_{l0} - 1, \tag{4.2a}$$

$$c_{\beta 1} = \chi k / A_v, \qquad c_{\beta 2} = w / A_v. \tag{4.2b}$$

Eq. (4.2a) can be rewritten in terms of $\Lambda = \beta_{l0}/2$ with corresponding coefficients $c_{1\Lambda} = 4c_{\beta 1}$ and $c_{2\Lambda} = 2c_{\beta 2}$. Eq. (4.2a) resembles the empirical fit found by Zhang et al. (2001) from radar and disdrometer data

$$p_l = c_{\Lambda 1Z}\Lambda^2 + c_{\Lambda 2Z}\Lambda - 1.957, \tag{4.3}$$

$c_{1\Lambda Z} = -1.6\times10^{-4}$ cm^{-2}, $c_{2\Lambda Z} = 0.1213$ cm^{-1}. A similar relation was suggested by Heymsfield (2003) for crystalline clouds

$$p_l = c_{\Lambda 1H}\Lambda^{c_{\Lambda 2H}} - 2, \tag{4.4}$$

$c_{\Lambda 1H} = 0.076$ cm$^{-0.8}$, $c_{\Lambda 2H} = 0.8$.

The estimates from (4.2a,b) with typical cloud parameters show that the value of $c_{\beta 1}$ has a smaller magnitude and is opposite in sign to $c_{\Lambda 1Z}$, hence, this relation is determined mostly by the coefficient $c_{\beta 2}$. This is in agreement with (4.3), which predicts a nearly linear relation except for very high values Λ, and with (4.4) where the power of Λ is 0.8, and the relation is close to linear. Thus, (4.2a,b) predict positive correlations between p_l, Λ and vertical velocities and is in agreement with experimental data and parameterizations. The increase in p_l and Λ with increasing w predicts narrower spectra in stronger updrafts and broader spectra in downdrafts, which is similar to the effect of stochastic condensation described in KC99a,b and Part 1. However, it should be emphasized that this analysis is just an illustration of possible applications of these analytical solutions and should be used with caution. The slope α_l in (4.1) and p_l - Λ relation (4.2a,b) are based on solutions with the presence of q_{ls}. In vigorous downdrafts, in the subcloud layer or near the surface where $q_{ls} \sim 0$, the solutions from section 3.4 can be used. Then (3.29) - (3.32) show that the slopes $\beta_{l0}(r)$ or $\Lambda(r)$ can be expressed as polynomials of p_l (equal to 1 in this case). These equations and the asymptotic analysis show that $\Lambda(r)$ is a 2nd order polynomial of p_l

if $v(r) << |w|$ and the slope is (3.32); such parameterization was suggested in Zhang et al. (2003a,b), and in Brandes et al. (2003), and a 3rd or 2.5 order polynomial if $v(r) >> |w|$ and the slope is (3.31).

Unfortunately, data on vertical velocities, turbulence coefficient, and presence of the small-size fraction are absent in the cited papers, which precludes a more detailed comparison. A verification of the relations (4.2a,b) would require simultaneous measurements of w, q_{ls}, q_{ll}, turbulent coefficient and the size spectra. However, these analytical solutions are consistent with the general findings from the experimental observations: since the slopes and indices are expressed through related quantities, this leads to existence of the p_l - Λ relations. At the same time, solutions in section 3 for various particular cases show that these relations cannot be universal, but should depend on the altitude and position of the measured spectra in cloud or below cloud base, and specifically the sign of w, values of k and α_l, and presence of q_{ls}. .

4.2 Example calculations for a crystalline cloud

The properties of snow spectra in a crystalline cloud are illustrated here in more detail. We select a generic case, chosen for illustration to mimic the profiles in similar clouds simulated in Khvorostyanov, Curry et al. (2001) and in Khvorostyanov and Sassen (2002) using a spectral bin model. The profiles for this case of $q_{ll}(z)$ and $\alpha_l(z)$ are shown in Fig. 1a,b along with the IWC of the small-size fraction q_{ls} and ice supersaturation, which are the same as described in Part 1, Fig. 1. The temperature decreases from about -5 ºC at the lower boundary to -60º at 12 km.

Shown in Fig. 2 are the vertical profiles of the slopes β_{l0} and Λ calculated for this case from (4.1). The generalized empirically-derived slope Λ for crystalline clouds from Platt (1997) is shown in Fig. 2b for comparison. The calculated slopes increase with decreasing temperature, although not linearly as predicted by the generalized experimental Λ but somewhat faster, especially above 7 km, since α_l and Λ are inversely proportional to q_{ls}, which decreases upward nonlinearly at these heights. However, the general agreement of the calculated and experimental curves is fairly good, both in magnitude and vertical gradients. This indicates that if a large ensemble of values of q_{ls} and q_{ll}, measured at various temperatures, are used to calculate α_l and Λ, then the results would converge to the experimental curve by Platt (1997).

An example of size spectra at ice subsaturation at the heights 4.8 - 6 km is shown in Fig. 3. The small-size fraction (Fig. 3a) was calculated with the generalized gamma distributions from section 4 of Part 1. In the spectral region from 6 to about 40 -50 μm, the spectra are almost linear in log-log coordinates, close to the Heymsfield-Platt inverse power laws with the indices increasing toward cloud top (to colder temperatures). At 50 -130 μm, the effect of the exponential tail dominates and the spectra have a maximum at ~ 100 - 130 μm that decreases with height.

The spectra of the large-size fraction (Fig. 3b) are calculated using (3.18) - (3.20). The spectra plotted in log-linear coordinates are nearly linear, i.e., close to the Marshall-Palmer exponents. The size-dependent slope $\beta_l(r)$ slightly decreases with r as predicted by the second term in (3.19), but the departure from linearity is small, the slope is determined mostly by β_{l0}. The composite spectra obtained by matching the small- and large-size fractions at r_0 = 72 μm (Fig. 3c) are seen to be bimodal. One can see that the calculated composite spectra and the experimental spectrum from Platt (1997) shown in Fig. 3d are in good agreement, having minima and maxima at similar positions (note the difference in radii and diameter scales in horizontal axes). The experimental and calculated values of f_l can be compared using the relation 1 $m^{-4} = 10^{-9}$ L^{-1} μm^{-1}; the maximum ~ 10^{11} m^{-4} in Fig. 3d corresponds to ~ 10^2 L^{-1} μm^{-1}, which is comparable to the maximum in Fig. 3c. In calculations here, the first bimodality occurs still within the small-size fraction. If the matching point was located at greater r_0 ~ 120 -150 μm, there would be the second region of bimodality at r_0 due to different slopes of the small- and large-size fractions; the bimodality is often observed in this region (e.g., Mitchell 1994, Mitchell et al. 1996), and polymodal spectra are also often observed (Sassen et al. 1989; Poellot et al. 1999).

The spectra in the layer 7.5 - 8.7 km with positive supersaturation are depicted in Figure 4. The indices of the small-size fraction (Fig. 4a) are positive (see Part I), and the spectra are monomodal gamma distributions with maxima at $r \sim 30 - 50$ μm. The portion of the spectra from ~10 to 50-60 μm in log-log coordinates is almost linear, i.e. it obeys the power law with indices slightly increasing with height. The large-size fraction (Fig. 4b), as seen in log-linear coordinates, represents the Marshall-Palmer distributions. The slopes are much steeper than in the lower layer and increase upward, i.e., the large-size spectra also become narrower at colder temperatures; these features are mostly due to the smaller q_{ls}, and the dependence $\beta_{l0} \sim q_{ls}^{-1}$. The composite spectra matched at 90 μm (Fig. 4c) exhibit features of bimodality, but weaker than in the lower layer. Now the bimodality occurs between the large- and small-size fractions rather than within the small-size fraction as was in Fig. 3 at $S < 0$. For comparison, given in Fig. 4d are the average size spectra from Lawson et al. (2006) measured in cirrus clouds at three temperatures. One can see that the calculated spectra (Fig. 4c) are similar to the observed spectra; in particular, they exhibit similar bimodality, become narrower at lower temperatures, and bimodality decreases and vanishes with increasing height. The reason for this is the decrease with height of IWC of the small fraction, slowing down accretion, and diminishing the large fraction. This analysis is consistent with observations (Sassen et al. 1989; Mitchell 1994; Platt 1997; Ryan 2000; Poellot et al. 1999) that bimodality is more pronounced in the lower layers.

Note that the spectra calculated at ice sub- and supersaturation are somewhat different. The experimental spectra, however, are usually presented without information about supersaturation, and may have been obtained from mixtures sampled in both sub -and supersaturated layers. This precludes a more detailed comparison at present and indicates that simultaneous measurements of the size spectra and supersaturation are desirable.

Fig. 5 shows the slopes $\beta_{le}(r)$ and size spectra calculated with (3.29) and (3.30) for the subsaturated subcloud layer where the small-size fraction has been evaporated. At small and large

r, the behavior of $\beta_{le}(r)$ is determined by (3.32) and (3.31) respectively. The slopes rapidly increase with radius, but the rate of this growth $\beta_{le}(r)/dr$ decreases at large r, which is determined by the increasing contribution from the second term with $v(r)$ in (3.30). This results in a rapid decrease in $f_l(r)$ towards the larger values of r. This feature has been observed in liquid clouds (e.g., Willis 1984), and, as Fig. 5 shows, can be pertinent also for subcloud layers of crystalline clouds. Since we consider here an example with spherical particles and asymptotic $v(r) \sim r^{1/2}$ (B_v = 1/2), the asymptotic behavior of the spectra is $f_l \sim \exp(-c_{l1}A_v r^{5/2})$ as described in section 3.4. For some crystal habits like aggregates or plates, the power B_v can be much smaller than 1/2 and closer to 0 (e.g., Mitchell 1996; KC02, KC05); then the decrease in f_l can be much slower and the tails in subcloud layer much longer.

5. Conclusions

The stochastic kinetic equations for the size spectra of liquid and crystalline precipitating particles are solved analytically for various assumptions. These solutions and their functional dependencies are used to explain and interpret observations and empirically-derived expressions for rain and snow size spectra such as the Marshall-Palmer distribution. The major results of this work can be summarized as follows.

The general solution of the stochastic kinetic equations for the large-size fraction (precipitating particles) is characterized by the product of an exponential term and a term that is an algebraic function of radius. The argument of the exponent consists of a slope of the Marshall-Palmer type and an additional integral that depends on the condensation and accretion rates, vertical velocities, turbulence coefficient, terminal velocity and vertical gradient of the liquid (ice) water content. The algebraic function is inversely proportional to the sum of the condensation and accretion rates and depends on the super- or subsaturation, terminal velocity and collection efficiency.

Several practically important particular cases are considered: a) terminal velocity as a linear function of radius; b) terminal velocity as a square root function of radius; c) accretion growth rate much greater than the condensation growth rate; and d) subcloud evaporation layer with very small or absent small-size fraction. The general solution is substantially simplified for these cases. The exponential part tends to the Marshall-Palmer exponent with the slope β_{l0}, but contains additional terms that make the slope radius-dependent and nonlinear, causing the spectra to decrease with radius faster than the MP exponent as observed in many experiments. This may influence the spectral moments, e.g., radar reflectivity and the relations between reflectivity and precipitation rates. The radius dependence of the algebraic function is weaker than that of the exponent, converts for sufficiently large radii to the power law, and the spectra also have the form of gamma distributions with the slope β_{l0} and index p_l, which can be positive or negative. However, these gamma distributions are different from those obtained for the small-size fraction (cloud particles) described in Part 1.

A simple expression is derived for the slope β_{l0} via 4 parameters: β_{l0} is proportional to the relative gradient of the liquid (ice) water content of the large-size fraction, to water or ice density, and inversely proportional to the collection efficiency and liquid (ice) water content q_{ls} of the small-size fraction. All of these parameters are available in cloud-scale and large-scale models, and these dependencies provide reasonable explanations for the observed features of β_{l0} with variations of each parameter. In particular, the inverse dependence, $\beta_{l0} \sim q_{ls}^{-1}$, provides an explanation of the observed strong inverse temperature dependence of β_{l0} since q_{ls} in general decreases with decreasing temperature.

Simple analytical expressions are also derived for the power indices p_l of the gamma distributions (shape parameters), which are expressed via the coefficients of the terminal velocity, the slopes β_{l0}, vertical velocity, and turbulent coefficient.

Based on these expressions for β_{l0} and p_l, a β_{l0} - p_l relation is derived for the case with terminal velocity proportional to radius as a 2nd order polynomial; this relation is similar to the empirical parameterizations based on radar and disdrometer data. The coefficients of this relation are expressed via vertical velocity, turbulent coefficient, and cloud liquid or ice water content.

These analytical solutions for the spectra of the large-size fraction and its parameters provide explanations for observed dependencies of the spectra on the temperature, turbulence, vertical velocities, liquid water or ice water content, and other cloud properties. The results are illustrated with calculations for a crystalline cloud. These analytical expressions can be used for parameterization of the size spectra and related quantities (e.g., optical properties, radar reflectivities) in bulk cloud and climate models and in remote sensing techniques. The solutions have been presented for liquid only and ice only size spectra. Treatment of mixed phase clouds would require simultaneous consideration of the small and large-size fractions of the drop and crystal spectra with account for their interaction (Findeisen-Bergeron process and transitions among the fractions) and is planned for the future work. Further work is needed to test the assumptions made in section 2 and to evaluate these expressions using observations.

Acknowledgments. This research has been supported by the Department of Energy Atmospheric Radiation Measurement Program, and NASA Modeling and Parameterization Program. Paul Lawson and Brad Baker are thanked for providing the data on the experimental size spectra and useful comments. The authors are grateful to three anonymous reviewers for the useful remarks that helped to improve the text. Jody Norman is thanked for help in preparing the manuscript.

Appendix A

Derivation of kinetic equation in continuous collection approximation

Following Voloshchuk (1984) and PK97, the stochastic collection equation is written as follows:

$$\left(\frac{\partial f(m)}{\partial t}\right)_{col,ls} = I_{gain} - I_{loss}\ , \tag{A.1}$$

$$I_{gain} = \frac{1}{2}\int_0^m K(m-m',m')f(m-m')f(m')dm'\ , \tag{A.2}$$

$$I_{loss} = f(m)\int_0^\infty K(m,m')f(m')dm'\ . \tag{A.3}$$

Here m, m', are the masses of the particles, $K(m,m')=\pi E_c(r,r')(r+r')^2|v(r)-v(r')|$ is the coagulation gravitational kernel, r and r' denote the radii of the drops (crystals) corresponding to m and m', $E_c(r,r')$ is the collection efficiency, $v(r)$ is the terminal velocity.

We represent the size spectrum as the sum of the two size fractions, $f(m) = f_s(m)\theta(m_0 - m) + f_l(m)\theta(m - m_0)$, where $\theta(x)$ is the Heaviside step function, $\theta(x) = 1$ at $x > 0$ and $\theta(x) = 0$ at $x < 0$. Substituting this decomposition into I_{gain}, we have the integral that contains in the subintegral expression 4 combinations of f_s and f_l:

$$I_{gain} = \frac{1}{2}\int_0^m K(m-m',m')[f_l(m-m')f_l(m') + f_s(m-m')f_l(m')$$

$$+ f_l(m-m')f_s(m') + f_s(m-m')f_s(m')]dm'\ , \tag{A.4}$$

By definition of the continuous collection approximation, the integrals of the 1st and 4th terms in the square brackets vanish. In the integral of the 3rd term, we introduce the new variable $m'' = m - m'$, then, with account for the symmetry of the kernel, $K(m - m'', m'') = K(m'', m - m'')$, the integral of the 3rd term becomes equal to the integral of the 2nd term, the coefficient 1/2 vanishes after summation of the two integrals, and the sum yields

$$I_{gain} = \int_0^{m_0} K(m-m',m') f_l(m-m') f_s(m') dm' . \tag{A.5}$$

The upper limit is determined by definition of $f_s(m')$, which also determines the upper limit in I_{loss}:

$$I_{loss} = f_l(m) \int_0^{m_0} K(m,m') f_s(m') dm' . \tag{A.6}$$

We assume some average value of $E_c(r,r')$ = const = E_c. Also, in the continuous growth approximation,

$$r >> r', \quad v(r) >> v(r'), \qquad K(m,m') \approx K(m,0) = \pi E_c r^2 v(r) . \tag{A.7}$$

Now we expand the subintegral expression in (A.5) for I_{gain} into the Taylor power series by the small parameter m' up to the term of first order

$$K(m-m',m') f_l(m-m') \approx K(m,0) f_l(m) - \frac{\partial}{\partial m}[K(m,0) f_l(m)] m' . \tag{A.8}$$

Substitution of this expression into (A.5) and using (A.7) yields

$$I_{gain} = K(m,0) f(m) \int_0^{m_0} f_s(m') dm' - \frac{\partial}{\partial m}[K(m,0) f(m)] \int_0^{m_0} dm' f_s(m') dm'$$

$$= f_l(m)[\pi E_c r^2 v(r) N_s] - \frac{\partial}{\partial m}[\pi E_c r^2 v(r) q_{ls} f_l(m)] . \tag{A.9}$$

Here, we used the normalization of $f_s(m)$

$$\int_0^{m_0} f_s(m') dm' = N_s , \qquad \int_0^{m_0} m' f_s(m') dm' = q_{ls} , \tag{A.10}$$

where N_s and q_{ls} are the number concentration and LWC (or IWC) of the small-size fraction. Since $m >> m'$, the kernel $K(m,m') \approx K(m,0)$ in (A.6) for I_{loss}, and can be removed outside the integral; then incorporating (A.7), I_{loss} becomes

$$I_{loss} = f_l(m)[\pi E_c r^2 v(r) \int_0^{m_0} f_s(m') dm'] = f_l(m)[\pi E_c r^2 v(r) N_s] , \tag{A.11}$$

where we again used the normalization (A.10). Now, comparison of (A.9) and (A.11) shows that the 1st term in I_{gain} (A.9) is equal to I_{loss} (2.11); thus they exactly cancel in (A.1) for $(\partial f_l/\partial t)_{col,ls}$, yielding

$$\left(\frac{\partial f_l(m)}{\partial t}\right)_{col,ls} = -\frac{\partial}{\partial m}[\dot{m}_{coag} f_l(m)], \tag{A.12}$$

where we denote

$$\dot{m}_{coag} \equiv \left(\frac{dm}{dt}\right)_{coag} = \pi E_c r^2 v(r) q_{ls}\,. \tag{A.13}$$

Thus, the collection rate $(\partial f_l/\partial t)_{col,ls}$ in approximation of continuous collection (A.12) can be derived directly from the Smoluchowski stochastic collection equation, represents a first order approximation to the full kinetic equation, and the term $\dot{m}_{coag}$ is the mass growth rate. Eq. (A.13) can be rewritten for $f_l(r)$ in terms of radii using the relation $f_l(m)dm = f_l(r)dr$, then substituting into (A.12) yields

$$\left(\frac{\partial f_l(r)}{\partial t}\right)_{col,ls} = -\frac{dm}{dr}\frac{\partial}{\partial m}[\dot{m}_{coag}\frac{dr}{dm} f_l(r)], \tag{A.14}$$

or

$$\left(\frac{\partial f_l(r)}{\partial t}\right)_{col,ls} = -\frac{\partial}{\partial r}[\dot{r}_{coag} f_l(r)] = -\chi\frac{\partial}{\partial r}[v(r) f_l], \tag{A.15}$$

where $\dot{r}_{coag}$ is the accretion radius growth rate

$$\dot{r}_{coag} = \dot{m}_{coag}\frac{dr}{dm} = \chi v(r)\,, \qquad \chi = \frac{E_c q_{ls}}{4\rho_w}. \tag{A.16}$$

Now the coagulation terms in Eq. (2.1) in the continuous collection approximation can be written in a simplified differential form using the Heaviside step function $\theta(x)$ as

$$\left(\frac{\partial f_{s,l}(r)}{\partial r}\right)_{col} = -\chi\frac{\partial}{\partial r}[v(r) f_l]\theta(r - r_0) - \sigma_{col} f_s(r)\theta(r_0 - r)\,. \tag{A.17}$$

The first term is the reduced gain I_{gain} for the large-size fraction. The second term is the reduced loss I_{loss} of the small size fraction, and the coefficient σ_{col} is defined below from the mass conservation.

If q_{ll} is the liquid (ice) water content of the large-size fraction, (A.15), (A.17) yield a simple parameterization of the accretion rate, dq_{ll}/dt, that can be used in bulk microphysical models, and is obtained by multiplying (A.15) by $(4/3)\pi\rho_w r^3$, and integrating over radius:

$$\frac{dq_{ll}}{dt} = \frac{4\pi\rho_w}{3}\int_0^\infty r^3\left(\frac{\partial f_l}{\partial t}\right)_{col} dr = -\frac{4\pi\rho_w}{3}\int_0^\infty r^3 \frac{\partial}{\partial r}(\dot{r}_{coag} f_l) dr\ . \qquad \text{(A.18)}$$

Here the lower limit is extended from r_0 to 0 noting that $f_l(r) = 0$ in this region. Integrating by parts and using (A.16), we obtain

$$\left(\frac{dq_{ll}}{dt}\right)_{col} = 4\pi\rho_w \int_0^\infty (\dot{r}_{coag} f_l) r^2 dr = q_{ls}\left(\pi E_c \int_0^\infty r^2 v(r) f_l dr\right) = \sigma_{col} q_{ls}\,, \qquad \text{(A.19)}$$

where we introduced the collection rate σ_{col} of the large-size fraction:

$$\sigma_{col} = \pi E_c \int_{r_0}^\infty r^2 v(r) f_l(r) dr\ . \qquad \text{(A.20)}$$

where σ_{col} is the same collection rate of the small-size fraction as defined in Part 1. Now, using (2.4) of Part 1 or (A.17) here for the loss of small particles,

$$\left(\frac{\partial f_s}{\partial t}\right)_{col} = -I_{loss} = -\sigma_{col} f_s\,, \qquad r < r_0\quad , \qquad \text{(A.21)}$$

multiplying it by $(4/3)\pi\rho_w r^3$ and integrating by radii, we obtain

$$\left(\frac{dq_{ls}}{dt}\right)_{col} = \frac{4\pi}{3}\rho_w \int_0^{r_0} r^3 \left(\frac{\partial f_s}{\partial t}\right)_{col} dr$$

$$= -\sigma_{col}\int_0^{r_0} \frac{4\pi\rho_w}{3} r^3 f_s dr = -\sigma_{col} q_{ls}\,, \qquad r < r_0 \qquad \text{(A.22)}$$

Comparison of (A.19) and (A.22) shows that if σ_{col} is defined by (A.20) for both small- and large-size fractions, then $(dq_{ls}/dt)_{col}$ = - $(dq_{ll}/dt)_{col}$, that is, the loss of mass of small-size fraction particles is equal in magnitude to the gain of the mass of large particles large-size fraction, and hence mass is conserved in continuous collection approximation.

Appendix B

Evaluation of the integrals in section 3.2 for $v(r) = A_v r$

If $v(r) = A_v r$, then $B_v = 1$ and I_1, I_2 in section 3can be rewritten as

$$I_1 = -\beta_{l0} bS \int_{r_1}^{r_2} \frac{dr}{bS + \chi A_v r^2}, \tag{B.1}$$

$$I_2 = \alpha_l (w - \alpha_l k) \int_{r_1}^{r_2} \frac{rdr}{bS + \chi A_v r^2}. \tag{B.2}$$

We introduce the notation

$$R = \left(\frac{b|S|}{\chi A_v} \right)^{1/2} = r \left(\frac{|\dot{r}_{cond}(r)|}{\dot{r}_{coag}(r)} \right)^{1/2}, \tag{B.3}$$

$$U = \beta_{l0} \frac{(\alpha_l k - w)}{2A_v}, \qquad Q = \frac{\beta_0 R}{2}, \tag{B.4}$$

Here the dimensions in CGS units are $[A_v] = \text{s}^{-1}$, $[R]$ = cm. Then I_1 for $S > 0$ can be rewritten as

$$I_1 = -\beta_{l0} R \int_{x_0}^{x} \frac{dx}{1 + x^2}, \tag{B.4}$$

where $x = r/R$, $x_0 = r_0/R$. This is the standard table integral, its evaluation yields

$$I_1 = -\beta_{l0} R[\arctan(r/R) - \arctan(r_0/R)] \tag{B.5}$$

For $S < 0$, the terms in denominator of (B.1) have different signs, thus I_1 can be rewritten as

$$I_1 = -\beta_{l0} R \int_{x_0}^{x} \frac{dx}{1 - x^2}, \tag{B.6}$$

This is also the standard table integral that is different for $|x| < 1$ and $|x| > 1$, i.e.,

$$I_1 = -\frac{\beta_{l0} R}{2} \ln \frac{1+x}{1-x}\Bigg|_{x_0}^{x}, \quad |x| < 1 \tag{B.7}$$

$$I_1 = -\frac{\beta_{l0} R}{2} \ln \frac{x+1}{x-1}\Bigg|_{x_0}^{x}, \quad |x| > 1 \tag{B.8}$$

For $r < R$, we have $|x| < 1$, and (B.7) is reduced to

$$I_1 = Q \ln\left(\frac{1-r/R}{1+r/R}\right)\Bigg|_{r_0}^{r}$$

$$= \ln\left[\frac{(1-r/R)(1+r_0/R)}{(1-r_0/R)(1+r/R)}\right]^{Q}, \qquad S < 0, \qquad r < R, \tag{B.9}$$

For $r > R$, we have $|x| > 1$, and (B.8) is reduced to

$$I_1 = Q \ln\left(\frac{r/R-1}{r/R+1}\right)\Bigg|_{r_0}^{r}$$

$$= \ln\left[\frac{(r/R-1)(r_0/R+1)}{(r_0/R-1)(r/R+1)}\right]^{Q}, \qquad S < 0, \qquad r > R, \tag{B.10}$$

The integral I_2 in (B.2) can be transformed for $S > 0$ as

$$I_2 = U \int_{x_0}^{x} \frac{d(x^2)}{x^2+1}, \qquad x = \frac{r}{R}, \tag{B.11}$$

and (B.11) is evaluated with the standard integral

$$I_2 = U \ln(1+x^2)\Big|_{x0}^{x} = \ln\left[\frac{1+(r/R)^2}{1+(r_0/R)^2}\right]^{U}, \qquad S > 0. \tag{B.12}$$

If $S < 0$, then $x < 0$ and I_2 can be transformed as

$$I_2 = U \int_{x_0}^{x} \frac{d(x^2)}{x^2-1}, \qquad x = \frac{r}{R}. \tag{B.13}$$

This integral is also standard and different at $x < 1$ and $x > 1$ and we get finally

$$I_2 = \ln\left(\frac{1-(r/R)^2}{1-(r_0/R)^2}\right)^U, \qquad S<0, \text{ and } r<R, \tag{B.14}$$

$$I_2 = \ln\left(\frac{(r/R)^2-1}{(r_0/R)^2+1}\right)^U, \qquad S<0, \text{ and } r>R. \tag{B.15}$$

These expressions for I_1 and I_2 are used in section 3.2 for the large-size fraction.

Appendix C

Evaluation of the integrals in section 3.3 for $v(r) = A_v r^{1/2}$

If $v(r) = A_v r^{1/2}$, then $B_v = 1/2$ and I_1, I_2 in section 3.3can be rewritten for $S > 0$ as

$$I_1 = -\beta_{l0} H I_{11}, \qquad I_{11} = \int_{t_1}^{t_2} \frac{dt}{1+t^{3/2}} \tag{C.1}$$

$$I_2 = \frac{V}{2} I_{21}, \qquad I_{21} = \int_{t_1}^{t_2} \frac{tdt}{1+t^{3/2}} \tag{C.2}$$

where

$$t = \frac{r}{H}, \qquad H = \left(\frac{b\,|\,s\,|}{\chi A_v}\right)^{2/3}, \qquad V = \frac{2\alpha_l (w-\alpha_l k) H^{1/2}}{\chi A_v}. \tag{C.3}$$

Here the dimensions in CGS units are $[A_v]$ = cm$^{1/2}$ s^{-1}, $[H]$ = cm, V is dimensionless. Introducing a new variable $x = t^{1/2}$, the integral I_{11} can be transformed into that given in Gradshteyn and Ryzhik (1994, hereafter GR94):

$$I_{11} = \int_{t_0}^{t} \frac{dt}{1+t^{3/2}} = 2\int_{x_0}^{x} \frac{xdx}{1+x^3}$$

$$= 2\left[-\frac{1}{6}\ln\frac{1-x+x^2}{(1+x)^2} + \frac{1}{\sqrt{3}}\arctan\frac{2x-1}{\sqrt{3}}\right]_{x_0}^{x}. \tag{C.4}$$

Then finally

$$I_1 = 2\beta_{l0}H\left\{\ln\left[\frac{(1+x)^2(1-x_0+x_0^2)}{(1+x_0)^2(1-x+x^2)}\right]^{1/6} - \frac{1}{\sqrt{3}}\left[\arctan\frac{2x-1}{\sqrt{3}} - \arctan\frac{2x_0-1}{\sqrt{3}}\right]\right\}. \quad (C.5)$$

Here and in subsequent equations, $x = (r/H)^{1/2}$.

The integral I_{21} in (C.2) can be evaluated with the same substitution, $x = t^{1/2}$,

$$I_{21} = \int_{t_0}^{t} \frac{tdt}{1+t^{3/2}} = 2\int_{x_0}^{x} \frac{x^3 dx}{1+x^3}$$

$$= 2\left[x - \frac{1}{3}\ln\frac{1+x}{(1-x+x^2)^{1/2}} - \frac{1}{\sqrt{3}}\arctan\frac{x\sqrt{3}}{2-x}\right]_{x_0}^{x}. \quad (C.6)$$

The last integral is from GR94. Substitution into (C.2) yields

$$I_2 = V\left\{x - \ln\left[\frac{(1+x)(1-x_0+x_0^2)^{1/2}}{(1+x_0)(1-x+x^2)^{1/2}}\right]^{1/3} - \frac{1}{\sqrt{3}}\left[\arctan\frac{x\sqrt{3}}{2-x} - \arctan\frac{x_0\sqrt{3}}{2-x_0}\right]\right\}, \quad (C.7)$$

For $S < 0$, I_1 can be transformed as

$$I_1 = -\beta_{l0}HI_{12}, \qquad I_{12} = \int_{t_0}^{t} \frac{dt}{1-t^{3/2}} \quad (C.8)$$

With the same substitution, $x = t^{1/2}$, the integral I_{12} can be reduced to that given in GR94

$$I_{12} = \int_{t_0}^{t} \frac{dt}{1-t^{3/2}} = 2\int_{x_0}^{x} \frac{xdx}{1-x^3}$$

$$= 2\left[-\frac{1}{6}\ln\frac{(1-x)^2}{1+x+x^2} + \frac{1}{\sqrt{3}}\arctan\frac{2x+1}{\sqrt{3}}\right]_{x_0}^{x} \quad (C.9)$$

Then finally

$$I_1 = 2\beta_{l0}H\left\{\ln\left[\frac{(1-x)^2(1+x_0+x_0^2)}{(1-x_0)^2(1+x+x^2)}\right]^{1/6} - \frac{1}{\sqrt{3}}\left[\arctan\frac{2x+1}{\sqrt{3}} - \arctan\frac{2x_0+1}{\sqrt{3}}\right]\right\}. \quad (C.10)$$

For $S < 0$, I_2 can be transformed as

$$I_2 = -\frac{V}{2} I_{22}, \qquad I_{22} = \int_{t_0}^{t} \frac{t dt}{1 - t^{3/2}} \tag{C.11}$$

With the same substitution, $x = t^{1/2}$, it can be transformed to the form given in GR94

$$I_{22} = 2 \int_{x_0}^{x} \frac{x^3 dx}{1 - x^3}$$

$$= 2 \left[-x + \frac{1}{3} \ln \frac{(1 + x + x^2)^{1/2}}{1 - x} + \frac{1}{\sqrt{3}} \arctan \frac{x\sqrt{3}}{2 + x} \right]_{x_0}^{x} . \tag{C.12}$$

Substitution into (C.11) yields:

$$I_2 = V \left\{ x - \ln \left[\frac{(1 + x + x^2)^{1/2} (1 - x_0)}{(1 + x_0 + x_0^2)^{1/2} (1 - x)} \right]^{1/3} - \frac{1}{\sqrt{3}} \left[\arctan \frac{x\sqrt{3}}{2 + x} - \arctan \frac{x_0\sqrt{3}}{2 + x_0} \right] \right\} . \tag{C.13}$$

These 4 integrals are used in section 3.3 for evaluation of the size spectra f_l for $v(r) = A_v r^{1/2}$.

References

Böhm, J. P., 1989: A general equation for the terminal fall speed of solid hydrometeors. *J. Atmos. Sci*., **46**, 2419-2427.

Brandes, E. A., G. Zhang, and J. Vivekanandan, 2003: An evaluation of a drop distribution-based polarimetric radar rainfall estimator. *J. Appl. Meteor.,* **42,** 652–660.

Brown, P. S., 1991: Parameterization of the evolving drop-size distribution based on analytic solution of the linearized coalescence breakup equation. *J. Atmos. Sci.,* **48**, 200-210.

——, 1997: Mass conservation considerations in analytic representation of rain drop fragment distribution. *J. Atmos. Sci.,* **54,** 1675–1687.

Cotton, W. R., R. A. Anthes, 1989: *Storm and Cloud Dynamics,* Academic Press, 883 pp.

Golovin, A. M., 1963: On the kinetic equation for coagulating cloud droplets with allowance for condensation. *Izv. Acad. Sci. USSR, Ser. Geophys.,* **10**, 949-953.

Feingold, G., S. Tzivion, and Z. Levin, 1988: Evolution of raindrop spectra. Part I: Solution to the collection/breakup equation using the method of moments. *J. Atmos. Sci.,* **45,** 3387–3399.

Gunn, K. L. S., and Marshall, J. S., 1958: The distribution with size of aggregates snowflakes. *J. Meteorol.,* 1**5**, 452-461.

Gradshteyn, I. S. and I. M. Ryzhik, 1994: *Table of Integrals, Series, and Products*, 5th ed., A. Jeffery, Ed., Academic Press, 1204 pp.

Heymsfield, A. J., 2003: Properties of tropical and midlatitude ice cloud particle ensembles. Part II: Application for mesoscale and climate models. *J. Atmos. Sci.,* **60**, 2592-2611.

Heymsfield, A. J. and C. M. R. Platt, 1984: A parameterization of the particle size spectrum of ice clouds in terms of the ambient temperature and the ice water content. *J. Atmos. Sci.,* **41**, 846-855.

Houze, R. A., P. V. Hobbs, P. H. Herzegh, and D. B. Parsons, 1979: Size distribution of precipitating particles in frontal clouds. *J. Atmos. Sci.,* **36**, 156-162.

Hu, Z., and R. C. Srivastava, 1995: Evolution of raindrop size distribution by coalescence, breakup, and evaporation: Theory and observations. *J. Atmos. Sci.,* **52,** 1761–1783.

Joss, J., and E. G. Gori, 1978: Shapes of raindrop size distributions. *J. Appl. Meteorol*, **17**, 1054-1061.

Kessler, E., 1969: On the distribution and continuity of water substance in atmospheric circulation. *Meteorol. Monogr.,* **10**, No.32, Amer. Meteor. Soc., 84 pp.

Khvorostyanov, V. I., and J. A. Curry, 1999a: Toward the theory of stochastic condensation in clouds. Part I: A general kinetic equation. *J. Atmos. Sci*., **56**, 3985-3996.

——, and ——, 1999b: Toward the theory of stochastic condensation in clouds. Part II. Analytical solutions of gamma distribution type. *J. Atmos. Sci*., **56**, 3997-4013.

——, and ——, 2002: Terminal velocities of droplets and crystals: power laws with continuous parameters over the size spectrum. *J. Atmos. Sci.,* **59,** 1872-1884.

——, and ——, 2005. Fall velocities of hydrometeors in the atmosphere: Refinements to a continuous analytical power law. *J. Atmos. Sci.,* **62**, 4343–4357.

——, and ——, 2008: Analytical solutions to the stochastic kinetic equation for liquid and ice particle size spectra in precipitating and non-precipitating clouds. Part I: small-size fraction. *J. Atmos. Sci.,* **65**, in press (this issue)

——, and K. Sassen, 2002: Microphysical processes in cirrus and their impact on radiation, a mesoscale modeling perspective, in *"Cirrus",* Oxford University Press, Eds. D. Lynch, K. Sassen, D. Starr and G. Stephens, 397-432.

——, J. A. Curry, J. O. Pinto, M. Shupe, B. A. Baker, and K. Sassen, 2001: Modeling with explicit spectral water and ice microphysics of a two-layer cloud system of altostratus and cirrus observed during the FIRE Arctic Clouds Experiment. *J. Geophys. Res*., *106*, 15,099-15,112.

Liu, Y., 1993: Statistical theory of the Marshall-Palmer distribution of raindrops. *Atmos. Environ.*, **27A**, 15-19.

Low, T. B., and R. List, 1982a: Collision, coalescence, and breakup of raindrops. Part I: Experimentally established coalescence efficiencies and fragment size distributions in breakup. *J. Atmos. Sci.,* **39,** 1591–1606.

——, and ——, 1982b: Collision, coalescence, and breakup of raindrops. Part II: Parameterization of fragment size distributions. *J. Atmos. Sci.,* **39,** 1607–1618.

Marshall, J. S., and W. M. K. Palmer, 1948: The distribution of raindrops with size. *J. Meteor.,* **5,** 165–166.

McFarquhar, G. M., 2004: A new representation of collision-induced breakup of raindrops and its implications for the shapes of raindrop size distributions. *J. Atmos. Sci.,* **61**, 777-794.

Mitchell, D. L., 1994: A model predicting the evolution of ice particle size spectra and radiative properties of cirrus clouds. Part I: Microphysics. *J. Atmos. Sci*., **51**, 797-816.

______, 1996: Use of mass- and area-dimensional power laws for determining precipitation particle terminal velocities. *J. Atmos. Sci*., **53**, 1710-1723.

______, S. K. Chai, Y. Liu, A. J. Heymsfield and Y. Dong, 1996: Modeling cirrus clouds. Part I: Treatment of bimodal spectra and case study analysis. *J. Atmos. Sci*., **53**, 2952-2966.

Passarelli, R. E., 1978a: An approximate analytical model of the vapor deposition and aggregation growth of snowflakes. *J. Atmos. Sci.,* **35**, 118-124.

______, 1978b: Theoretical and observational study of snow-sized spectra and snowflake aggregation efficiencies. *J. Atmos. Sci.,* **35**, 882-889.

Platt, C. M. R., 1997: A parameterization of the visible extinction coefficient in terms of the ice/water content. *J. Atmos. Sci.,* **54**, 2083-2098.

Pruppacher, H. R., and Klett, J. D., 1997: *Microphysics of Clouds and Precipitation*, 2nd Edition, Kluwer, 997 pp.

Rogers, R. R, 1979: A *Short Course in Cloud Physics*. 2nd ed., Pergamon Press, 235 pp.

Ryan, B. F, 2000: A bulk parameterization of the ice particles size distribution and the optical properties in ice clouds. *J. Atmos. Sci.,* **57**, 1436-1451.

Sassen, K., D. O'C. Starr, and T. Uttal, 1989: Mesoscale and microscale structure of cirrus clouds: Three case studies. *J. Atmos. Sci.,* **46**, 371-396.

Scott, W. T., 1968: Analytic studies of cloud droplet coalescence. *J. Atmos. Sci.,* **25**, 54-65.

Seifert, A., 2005: On the shape-slope relation of drop size distributions in convective rain. *J. Appl. Meteorol.* **44**, 1146-1151.

Srivastava, R., C., 1971: Size distribution of raindrops generated by their breakup and coalescence. *J. Atmos. Sci.,* **28**, 410- 415.

——, 1978: Parameterization of raindrop size distribution. *J. Atmos. Sci.,* **35**, 108 - 117.

——, 1982: A simple model of particle coalescence and breakup. *J. Atmos. Sci.,* **39**, 1317 - 1322.

______, and R. E. Passarelli, 1980: Analytical solutions to simple models of condensation and coalescence. *J. Atmos. Sci.*, **37**, 612-621.

Ulbrich, C. W., 1983: Natural variations in the analytical form of the raindrop size distribution. *J. Climate Appl. Meteor.,* **22,** 1764–1775.

Verlinde, J., P. J. Flatau, and W. R. Cotton, 1990: Analytical solutions to the collection growth equation: comparison with approximate methods and application to cloud microphysics parameterization schemes. *J. Atmos. Sci*., **47**, 2871-2880.

Voloshchuk, V. M., 1984: *The Kinetic Theory of Coagulation.* Hydrometeoizdat, Leningrad, 283 pp.

Willis, P. T., 1984: Functional fits to some observed drop size distributions and parameterization of rain. *J. Atmos. Sci.,* **41**, 1648-1661.

Zawadski, I., and de M. A. de Agostinho, 1988: Equilibrium raindrop size distributions in tropical rain. *J. Atmos. Sci.,* **45**, 3452 - 3459.

Zhang, G., J. Vivekanandan, and E. A. Brandes, 2001: A method for estimating rain rate and drop size distribution from polarimetric radar measurements. *IEEE Trans. Geosci. Remote Sens.,* 39, 830-841.

——, ——, and E. A. Brandes, 2003a: Constrained gamma drop size distribution model for polarimetric radar rain estimation: Justification and development. *Preprints, 31st Int. Conf. on Radar Meteorology*, Seattle, WA, Amer. Meteor. Soc., 206-225.

——, ——, ——, R. Meneghini, and T. Kozu, 2003b: The shape- slope relation in observed gamma raindrop size distributions: Statistical error or useful information? *J. Atmos. Oceanic Technol.,* 20, 1106-1119.

Figure captions

Fig. 1. Profiles for calculations of the spectra of the large fraction: (a) IWC of the large fraction (solid circles), and of the small fraction in the baseline case (open circles) and with doubled IWC (open diamonds); (b) parameter α_l; (c) ice supersaturation.

Fig. 2. (a) Exponential slope β_{l0} and (b) Λ_{l0} of the size spectra of the large-size fraction calculated with the IWC of small-size fraction q_{ls} (circles) and $2q_{ls}$ (diamonds) as described in Part 1. The generalized experimental slope for crystalline clouds from Platt (1997) and Ryan (2000) recalculated from the temperature to height with the average lapse rate 6.5 ºK km^{-1} is plotted in (b) with triangles.

Figure 3. Crystal size spectra by radii *r* (L^{-1} μm^{-1}) at ice subsaturation at the heights in km indicated in the legends and the temperatures decreasing from -14.9 ºC at 4.8 km to -22.15 ºC at 6.0 km. (a) small fraction; (b) large fraction; (c) composite; (d) generalization by Platt (1997) of the observed crystal size spectra by long dimension *D* (m^{-4}) in the temperature interval -25 ºC to -30 ºC. Note different normalization of the spectra and axes scales in (a)-(c) by radius and (d) by diameter.

Fig. 4. Crystal size spectra by radii (L^{-1} μm^{-1}) at ice supersaturation at the heights indicated in the legends. (a) for the small fraction extended to 200 μm; (b) for the large fraction; (c) composite spectra; and (d) experimental spectra in cirrus clouds from Lawson et al. (2006) at 3 indicated temperatures.

Fig. 5. (a) Slopes and (b) size spectra in the subcloud layer with zero IWC of small-size fraction q_{ls} at the heights (km) indicated in the legends.

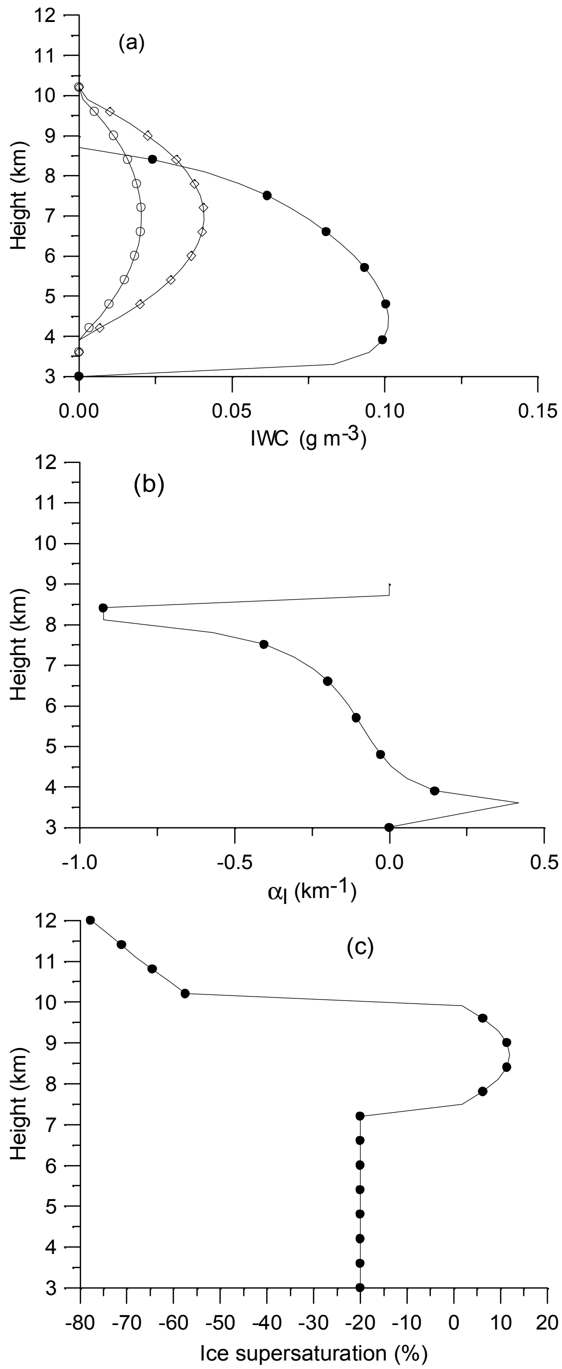

(a)
Height (km)
IWC (g m-3)
0.00
0.05
0.10
0.15
(b)
Height (km)
αI (km-1)
-1.0
-0.5
0.0
0.5
(c)
Height (km)
Ice supersaturation (%)
-80
-70
-60
-50
-40
-30
-20
-10
0
10
20

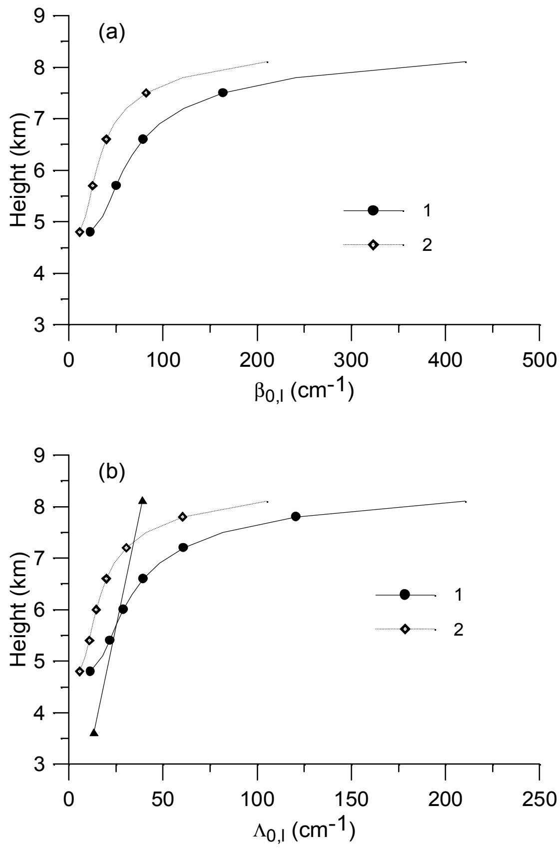

(a)
Height (km)
β0,l (cm-1)
1
2
(b)
Height (km)
Λ0,l (cm-1)
1
2

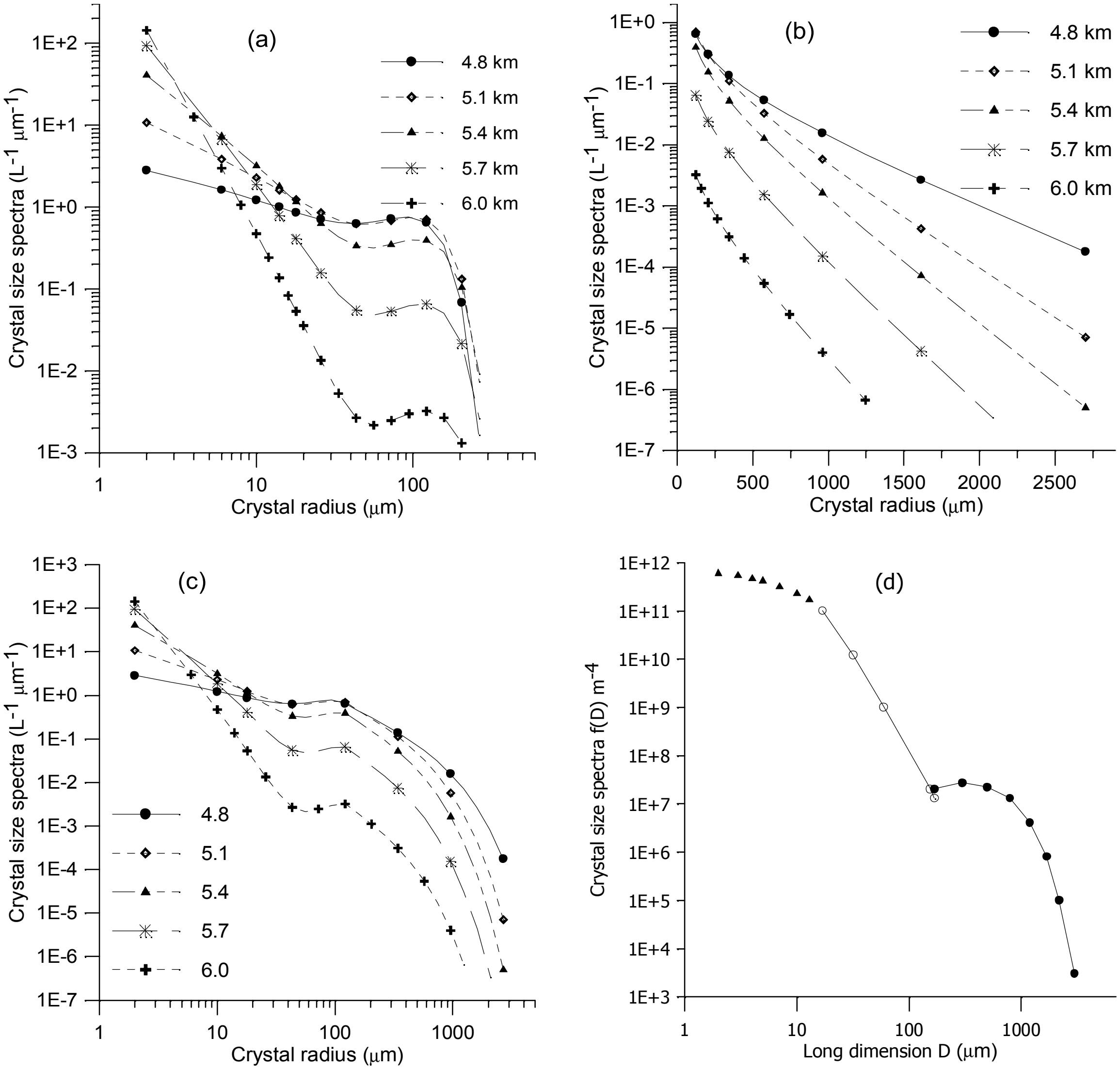
(a)
4.8 km
5.1 km
5.4 km
5.7 km
6.0 km
Crystal size spectra (L-1 μm-1)
Crystal radius (μm)
(b)
4.8 km
5.1 km
5.4 km
5.7 km
6.0 km
Crystal size spectra (L-1 μm-1)
Crystal radius (μm)
(c)
4.8
5.1
5.4
5.7
6.0
Crystal size spectra (L-1 μm-1)
Crystal radius (μm)
(d)
Crystal size spectra f(D) m-4
Long dimension D (μm)

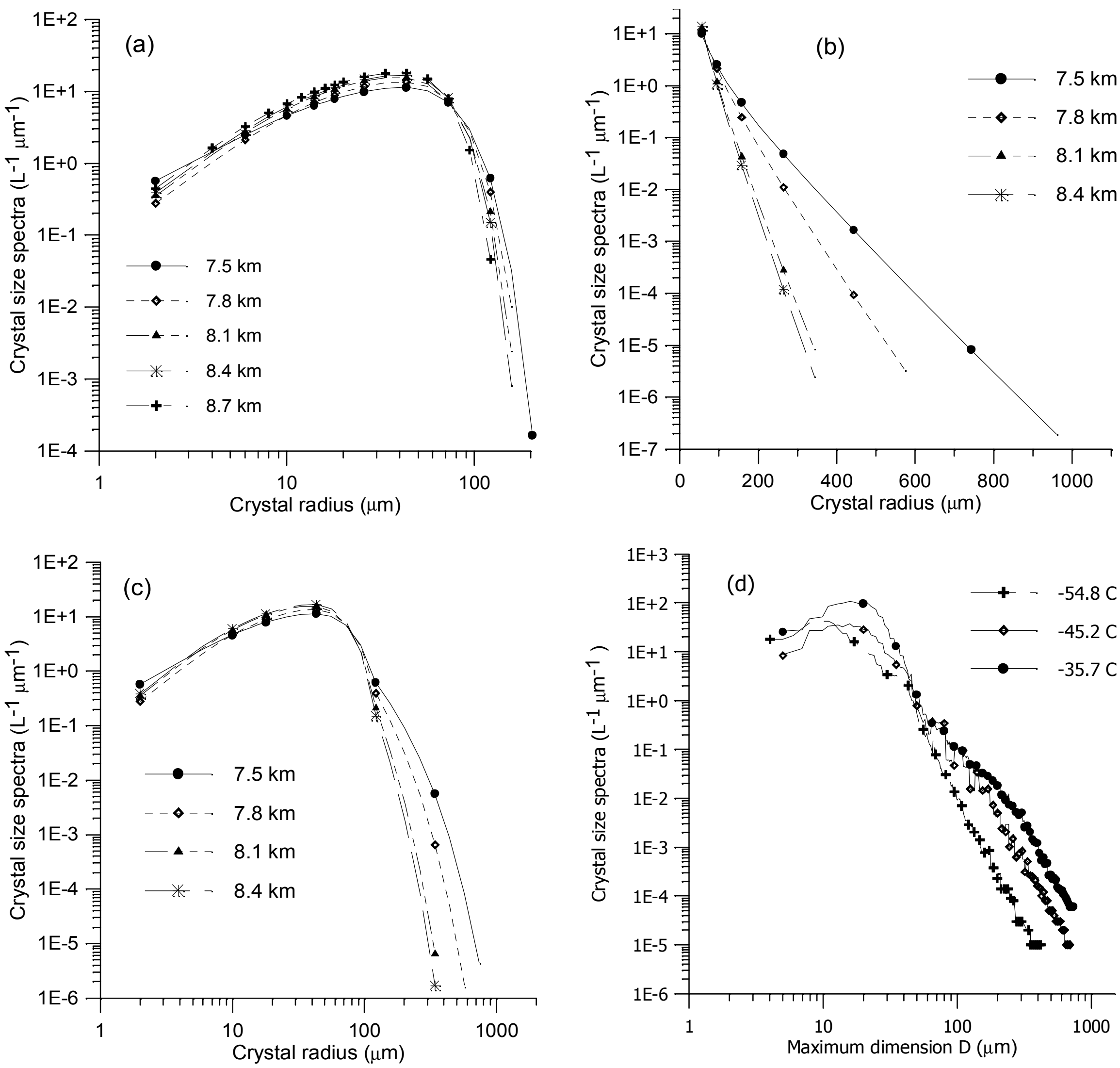

(a)
Crystal size spectra (L^{-1} μm^{-1})
Crystal radius (μm)
7.5 km
7.8 km
8.1 km
8.4 km
8.7 km
(b)
Crystal size spectra (L^{-1} μm^{-1})
Crystal radius (μm)
7.5 km
7.8 km
8.1 km
8.4 km
(c)
Crystal size spectra (L^{-1} μm^{-1})
Crystal radius (μm)
7.5 km
7.8 km
8.1 km
8.4 km
(d)
Crystal size spectra (L^{-1} μm^{-1})
Maximum dimension D (μm)
-54.8 C
-45.2 C
-35.7 C

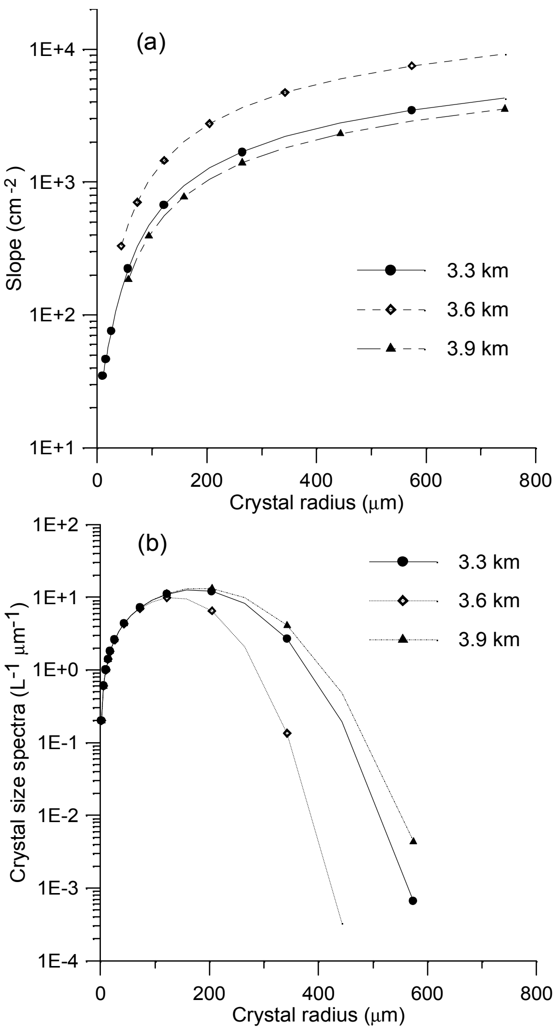

(a)
Slope (cm-2)
1E+1
1E+2
1E+3
1E+4
0
200
400
600
800
Crystal radius (μm)
3.3 km
3.6 km
3.9 km
(b)
Crystal size spectra (L-1 μm-1)
1E-4
1E-3
1E-2
1E-1
1E+0
1E+1
1E+2
0
200
400
600
800
Crystal radius (μm)
3.3 km
3.6 km
3.9 km